uc3m | Universidad Carlos III de Madrid

Aerospace Engineering
2017/2018

Final Degree Project

An Experimental Study of the Effect of Tubercle Leading Edge on the Performance of NACA Airfoils

---

Author
Carlos María Moya Sanz

Tutor
Carlos Sanmiguel Vila

Leganés, February 2018

Acknowledgment

I would like to express my very great appreciation to Carlos Sanmiguel who has guided and help me with enthusiasm through this exciting project.

I would like to offer my special thanks to Dr. Stefano Discetti for giving me the opportunity of perform this final degree thesis. Assistance provided by Carlos Cobos and Victor Criado was greatly appreciated.

To my family and girlfriend for supporting and put up with me in difficult moments and encourage me to continue my academical studies.

Abstract

This thesis presents a study on tubercle leading edge configurations inspired in the Humpback Whale flipper. Is expected that stall appears at a higher angle of attack in a modified wing than in an unmodified wing. First a literature review is done and based on this review, 3 different configurations of wings are selected, varying between them the amplitude and wavelength of the tubercles. In order to perform this analysis an installation for measurement of forces is designed and built, together with the 3 modified wings and the unmodified one. The experiments are performed in a wind tunnel at Re=8.2x10^5. To support the results obtained in the tunnel, a simulation of the modified NACA 0012 with the best behavior is performed in SimScale, a CFD platform.

From the experiments is obtained that wings which have tubercle leading edge, present better aerodynamics behavior in the post stall region, because for the three configurations, is seen that stall appears later and softer than the unmodified NACA 0012. Comparing the models is seen that the one which presents the smoothest stall is the wing with the smallest size of tubercles. That modified wing is analyzed in SimScale obtaining again a delay in stall in comparison with the unmodified NACA 0012. In terms of efficiency is seen that tubercles penalize the pre stall region, in return, post stall region presents better values of efficiency, being in that case the wing with medium size of tubercles the one with best aerodynamic efficiency performance.

Finally, thanks to the results and conclusions obtained, the installation is validated.

Key words

Tubercle Leading Edge; Separation; Biomimetic; Experimental Aerodynamics; CFD

Contents

List of Figures

List of Tables

Nomenclature

α	Angle of attack, [°]
α_e	Effective angle of attack, [°]
β^*	Model constant [-]
δX_i	Uncertainty
Δy	First layer thickness, $[m]$
δ	Displacement thickness, $[m]$
ϵ_{SB}	Solid blockage [-]
ϵ_T	Total blockage [-]
ϵ_{WB}	Wake blockage [-]
Γ	Vortex intensity [-]
λ	Tubercle wavelength, $[m]$
μ	Dynamic viscosity, $[kg/ms]$
ν	Kinematic viscosity, $[m^2s]$
ω	Specific turbulence dissipation rate [-]
$\overline{u'}$	Mean fluctuating velocity, $[m/s]$
ψ	Sinusoid phase, $[rad]$
τ_1	Wind tunnel shape factor [-]
τ_W	Wall shear stress, $[Pa]$
A	Tubercle Amplitude, $[m]$
c	Chord, $[m]$
C_D	Drag coefficient [-]
C_L	Lift coefficient [-]
C_μ	$k-\omega$ model parameter [-]
C_{D0}	Minimum drag [-]
C_{Di}	Induced Drag [-]
C_p	Pressure coefficient [-]
F	Force, $[N]$

K	Turbulent kinetic energy, $[m^2/s^2]$
K_1	Body shape factor [-]
L	Characteristic length ,$[m]$
P	Pressure, $[Pa]$
q	Dynamic pressure, $[Pa]$
q_C	Corrected dynamic pressure, $[Pa]$
q_u	Uncorrected dynamic pressure, $[Pa]$
R	Ideal gas constant, $[J/Kg^{-1}K^{-1}]$
Re	Reynolds number [-]
S	Wing surface, $[m^2]$
T	Temperature, $[K]$
t	Thickness, $[m]$
U_∞	Free stream velocity, $[m/s]$
w	Vertical velocity (downwash), $[m/s]$
y^+	Yplus [-]

1 Introduction

Aircraft industry has always been a very dynamic industry continuously changing and growing, it can be demonstrated taking into account that the first flight was performed in a little more than a century ago and nowadays thousands of flights are performed daily in a regular way over the world. This dynamism is these days accentuated thanks to the huge amount of technical progress in this field, as simulations programs, mathematical softwares, powerful computers, accurate measurements instruments, etc.

It is important to notice that these changes are influenced by the circumstances and requirements of the time. For example in 1938 appears the Boeing 307 'Stratoliner' being the first pressurized commercial aircraft, increasing safety in flight because at high altitudes adverse environmental conditions can be avoided. Over years, continuous evolutions improving power, safety, maneuverability and comfort has been made, but these days one of the most important aspect to enhance is the efficiency. It is a proven fact that climatic change is happening and aviation produces 2% of global greenhouse gas. To get some idea of this value, if global aviation was a nation, it will be in top 10 of most contaminants countries [1]

European Union is committed with that fact, so it funded a program called Clean Sky 2 in the frame of the Horizon 2020 Plan whose main targets are:

- Reduce fuel consumption and CO_2 emissions by 50% per passenger kilometer
- Reduce NOx emissions by 80%

Those reductions must be fulfilling between years the 2000 and 2020.[2]

Pollution is not the only concern of airplanes efficiency, commercial airlines has very high expenses in fuel, so they look for ways of reducing waste in kerosene.

There are many ways of saving fuel, for example making engines more efficient in cruise phase which is the largest one, or increasing the aerodynamic efficiency of the airplane. This tendency can be seen in new models of the two main aerospace manufacturers. The A320 NEO and 737 MAX whose main characteristic is the improvement in efficiency. Those aircrafts are arriving to the state of the art limit, it is for this reason that configurations known as non-conventional are appearing, for example the joined wings with diamond shape.

Next, some fundamental concepts are going to be explained, to have a better understanding of the project.

1.1 Biomimetics

There exist an interesting discipline called *Biomimetics* that consists on imitation of natural models, systems and elements for the purpose of solving human problems [3]. Nature progress is the result of hundreds of thousands years of iterative evolution so is the perfect source of ideas.

The most famous case is the origin of Velcro, it was created by a Swiss alpinist who notice that the burrs of the alpine thistle get stuck with great force to his dog skin. He created the Velcro technology imitating the hook shape of the tip of this thistle [4]. But *Biomimetics* has an important disadvantage because organisms usually operates with different set of principles than technology. This is due to engineering systems are created by decision-making while natural bodies are the results of a Darwinian process of natural selection. For example aircrafts speed and payload are huge in comparison with birds. Key step in *Biomimetics* consists in look for an overlap in size and performance between the system and organism [5]. For instance flapping wings have been implemented into micro UAVS imitating the flutter o birds.

1.2 Marine mammals

It is known that marine mammals can perform very agile movements, so if engineers were capable of implement the aspects that allow these agile movements, airplanes characteristics could be improved. For example, dolphins can change the curvature of its fluke which has the same effect of increasing or decreasing the camber of the fluke. This change enables dolphins to do the acrobatics jump which characterize them.

Frank E Fish was fascinating by the faster tight turning and jumps of the humpback whale (*Megaptera Novaeangliae*) in spite of its huge weight and size [6]. He realized that all humpback whales have a kind of protuberances in its flipper that could be the reason of these spectaculars movements and if this tech could be applied to a wing, maybe its features will be enhanced. This effect is termed **"Tubercle Effect"**. Through some experiments, in a modified wing, it has been proved that stall region appears at a higher angle of attack than in an unmodified wing, ending in a greater efficiency. The dimensions of a typical Humpback Whale are 16 meters long and weight around 36000 kg [7]. One can appreciate that these values are applicable to a real aircraft, so the drawback of *Biomimetics* disappears.

Figure 1: Humpback whale flipper. Image taken from [6]

Sea animals have evolved along centuries trying to survive adapting to marine environment. In order to achieve it, these species have developed different mechanisms which allows active or passive control flow over their body. Active control consist on enhance hydrodynamic characteristics by movements of appendices, fins or even their skins. An example of active control is the case of dolphins previously explained. On the other hand, passive control flows is based on improve hydrodynamic characteristics by the own morphology of the body .The case of study for this work is framed in passive flow control [6].

1.3 Streamwise vortices

Main cause of delaying stall in a modified wing is attributed to a generation of streamwise vortices, which improve the momentum exchange in the boundary layer. In other words, boundary layer is energized, consequently, separation is delayed. A practical example of streamwise vortices can be found in golf balls. Those balls present a kind of bumps which acts as vortex generators, having a better performance than a smooth ball.[8]

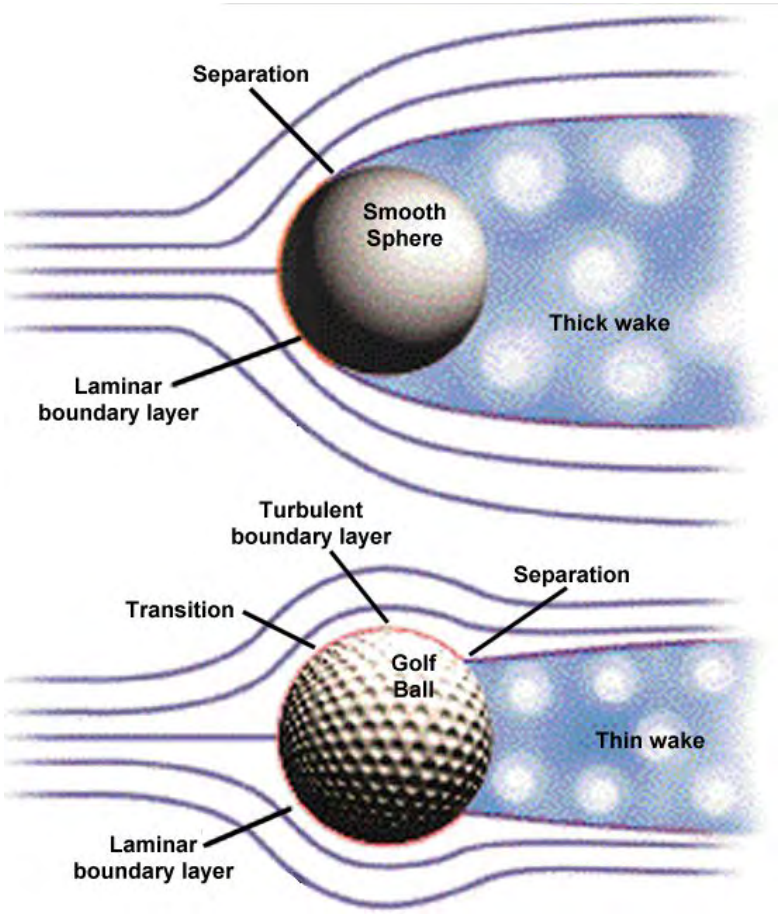

Figure 2: Golf balls aerodynamics. Image taken from [8]

Before explaining how vortices works, is important to know about the creation of that vortices. Two different reasons are giving:

- Leading edge of modified wings are characterized by tubercles, so if an alone tubercle is selected can be seen that it is like a small delta wing. In leading edge of delta wings vortices appear due to flow passes from pressure side to suction side. [9]
- Kelvin-Helmholtz instability can be used to predict transformation of a fluid in turbulent. It produces tubes of vorticity normal to the leading edge surface, but due to vorticity itself, these tubes are rotate into streamwise direction. [10]

In Figure 3 can be seen that a counter-rotating streamwise vortices must appears in a trough. Taking advantage of the explanation of tubercle as a delta wing, it is seen how for one side of tubercle, flows goes clockwise while for the other side, goes counter-clockwise. Due to tubercle modifications, leading edge will suffer strong pressure gradient resulting in the production of vorticity as previously explained. Those vortices will produce a downwash at peaks and upwash at the troughs which will vary the effective angle of attack.

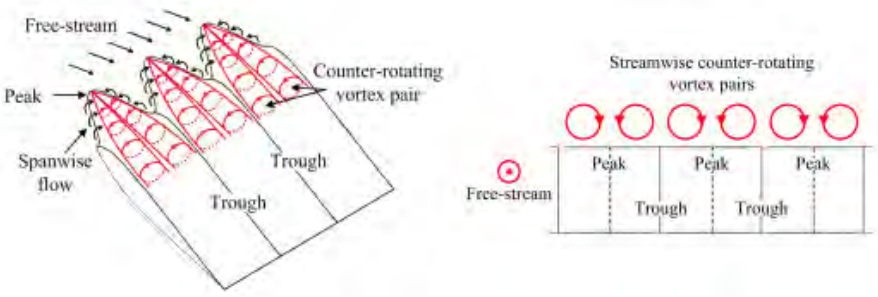

Figure 3: Streamwise vortices formation. Image taken from [11]

Once is determine the presence of streamwise vortices, spanwise momentum at the wall formula will relate it, with the existence of pressure variation along span direction.

$$\rho v_w \cancelto{0}{\left.\frac{\partial v}{\partial x}\right|_0} + \left.\frac{\partial p}{\partial y}\right|_{z=0} - \cancelto{0}{\frac{\partial \mu}{\partial z}} \left.\frac{\partial v}{\partial z}\right|_{z=0} = \mu \left.\frac{\partial^2 v}{\partial z^2}\right|_{z=0} \tag{1}$$

The elements eliminated in the previous equation are produced by no penetration condition $v_w = 0$ and constant dynamic viscosity μ =cte.

Vortices have a complex pattern, so in the next section it is going to be explained.

1.4 Vortices flow pattern

Up to this point it is known that tubercles generate vortices, which create a pressure gradient in spanwise direction and boundary layer stall will be delayed.

Suction peak occurs at different location in troughs and peaks (troughs and peaks are defined in Figure 3, because thickness and chord values are not equal for each case, being that point further aft for trough than peaks. That point will affect the position where adverse pressure gradient appears. Appearance of adverse pressure gradient leads to a compression of vortices, increasing its cross-sectional area and reducing the vorticity magnitude along chord direction.

Next figure shows clearly the presence of counter rotating vortices (being red, positive vorticity and blue, negative vorticity). Notice that maximum vorticity magnitude is similar for both counter rotating vortices. In the image, compression of vortices can be seen, increasing its cross-sectional area, but compression phenomenon and vorticity reduction is not only caused by different location of suction peak. In figure 3 can be notice a presence of secondary vortices with an opposite sign of vorticity over primary vortices, which will reduce vorticity magnitude. However, circulation increases in chordwise direction. This occurs because separation appears earlier in a trough than in a peak. So behind a trough, a small adverse pressure gradient must appears.

Behind trough vortices line, flow lifts up from wing surface forming a canopy of vorticity, where separation occurs. In the edge of that canopy there exists vortex sheets that will affect streamwise vortices, increasing circulation of primary vortices as previously mentioned. After, the flow is reattached to the wing. [12]

The demonstration that circulation increases with streamwise direction is very important because this behavior has been also observed in delta wings, so theory of tubercles behaves as delta wings gain strength.[13]

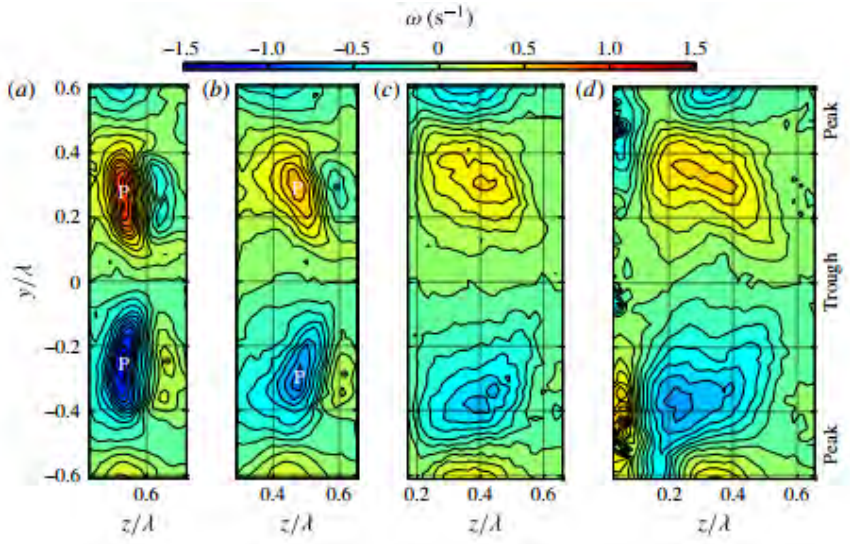

Figure 4: Flow pattern for different chord positions: a)=x/c=0.4, b)=x/c=0.6, c)=x/c=0.8, d)=x/c=1. Image taken from [12]

This pattern of vortices has also been observed in experiments using Particle image velocimetry (PIV). [11]

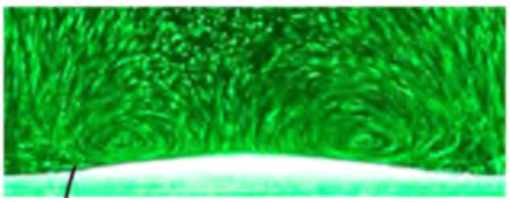

Figure 5: PIV visualization of counter rotating vortices.Image taken from [11]

1.5 Potential aerodynamic model

How tubercles performs is still a topic of discussion. Ernst Van Nierop said that it is not possible that bump act as vortex generator since the amplitude and wavelength of the tubercles are much greater than the boundary layer thickness. He proposed, in a potential aerodynamic model, that peaks of tubercles modify pressure distribution in such a way that behind peaks separation is delayed. Using Kutta condition the circulation can be determined as:

$$\Gamma = -\pi U_\infty \left(c + \frac{4t}{3\sqrt{3}} \right) \alpha^e + O((\alpha^e)^3, t^3) \tag{2}$$

Looking previous equation can be notice that circulation have a dependence on chord (c) and thickness (t). Due to the shape of profiles, that change in chord and thickness along span, circulation will also vary along span. That fluctuation in circulation will produce a different downwash at each point of the span, ending in a different affective angle of attack at each section.

$$\alpha^e = \alpha - \frac{w}{U_\infty} \tag{3}$$

Being w the downwash and U_∞ the free stream velocity.

Potential theory does not take into account viscosity so is not valid for analysis near walls, where boundary layer appears, governed by viscosity effects. To characterize the stall, next criteria is apply, using the non-dimensional pressure coefficient.

$$F(x) = C_p \left(x \frac{dC_p}{dx} \right)^{1/2} (10^{-6} Re)^{-1/10} \tag{4}$$

Depending on the value of $F(x)$ separation point can be calculated.

As previously said, Van Nierop try to show that tubercles delay separation by altering pressure distribution along wing, and he proved it with the potential theory and stall characterization above shown. [14]

As can be seen there exist two main currents for the explanation of how tubercles perform in the flow.

- Tubercles act as vortex generators
- Tubercles create a pressure variation along wing

Both mechanisms finally end in the same consequence which is appearance of turbulent flow, delaying stall.

1.6 Industrial application

In the present, tubercles have been applied in real structures such as submarines. The Umpty Squash presents in 2005 a submarine with tubercles in the rudder and dive planes in the International Submarine Races. Also tubercles can be found in the leading edge of surfboard skeg of the company Fluid Earth. But maybe the most important application that can be given to tubercles is the increase of power generation in wind turbines with tubercles in the blades for moderate wind speeds (7m/s-16m/s) with respect to unmodified blades.

The passive nature of leading-edge tubercles may be particularly appropriate for application in wings involved with the aerodynamics of high angle of attack. Such situations occur in general aviation aircraft and in helicopter rotor blades. As tubercles delays stall at high angles of attack, their use in conventional aircraft may allow replacement of flaps and slots reducing the weight of the airplane and increasing fuel economy. [5]

1.7 Objectives

The objectives of the project are: creation and validation of force measurement installation and study the behavior of a tubercle leading edge wing.

Develop an installation that allows measurement of forces in a wind tunnel. Is important to remark, that this is the first time that forces are measured in this wind tunnel.

Validate that installation studying the behavior of a tubercle leading edge and comparing the results obtained with the literature review.

At the same time, the aerodynamics characteristics of three modified tubercles leading edge wings are going to be studied in the wind tunnel (Forces, flow pattern, pressure fields and stall angle of attack) comparing it with an unmodified wing and the literature review. The configuration of the tubercles have been selected following past experiments and analysis.

In order to present clearly all the procedures followed and conclusions obtained, the project is divided in five main parts:

- Experimental procedure. Sections 2-7. At this part, all aspects related with experimental set-up and important considerations for wind tunnel experiments are developed.
- Experimental results. Section 8. Analysis of obtained data and comparison.

- Computational Fluid Dynamics. Section 9. Development of a CFD analysis to support and corroborate experimental analysis.
- Regulatory framework and socio-economic environment. Section 10. Aspects related to prevention law, costs, license of software and patents.
- Conclusion. Section 11.

Once the introduction and objectives are presented, is possible to start the explanation of the project procedure.

2 Experimental Set-Up

This section will be devoted to describe all process and steps follow to prepare and perform the experimental procedure.

Before making any design and wing configuration is necessary to perform a bibliographic research of previous experiments.

2.1 NACA and Reynolds number selection

When selecting an airfoil, two main NACA are selected, trying to represent as much accuracy as possible a Humpback whale flipper. The most similar one is NACA 634-021 [15] [16] [17] . First digit (6) denotes that this airfoil is designed for a greater laminar flow than four and five digits. Second number (3) gives the position of minimum pressure with respect chord, 0.3c. Number 0 denotes that airfoil is symmetric and finally, the 21 establish value of maximum thickness (0.21c).

It is important to bear in mind that thickness location has an important influence in tubercle effect. Profiles with maximum thickness located at 50% of the chord, tubercles have negligible effect on the lift performance in the prestall and are beneficial in poststall. Nevertheless NACA 0012, which has a maximum thickness of located at 30% of chord, has better performance in poststall, that involves worst lift performance in prestall. [20]

NACA 0012 is selected for the experimental study. The reason why this profile has been chosen is the existence of a great amount of experiments and papers to compare and validate [21] [22] [23]. Is a profile standardized for experimental aerodynamics and well characterized.

Symmetric NACA is used to have the possibility of sweep angles from negative to positive. Thinner NACA was not selected, for example NACA 0006, because is typical section for supersonic flow.

Typically, Reynolds number in wind tunnels in past studies was about 1.2 x 10^5 - 2 x 10^5. That can be considered low Reynolds number. But for this project Reynolds number is even lower, reaching a **Re=8.2 x 4**. This value is limited by the maximum power that wind tunnel can reach

Researchers found that at Re=1.5x10^4 tubercles starts to have effects in flow over wings.

2.2 Wing configuration

Once NACA profile is chosen, next step is select a proper configuration of tubercles to study its effect and the difference between configurations.

Regarding bibliography of past experiments, a very important non-dimensional parameter appears; the **amplitude to wavelength ratio**

$$\frac{A}{\lambda} \tag{5}$$

Along numerous studies, this value has determined the behavior of lift along wing. As smaller is that ratio, greater maximum lift is reached, but the stall region is not smooth. It can have sense because small ratio means small amplitude or bigger wave length which after all is similar to an unmodified wing. However bigger values of amplitude wavelength ratio ends in a smaller maximum lift but a smooth entry in stall regime. [17]

Taking this into account three different configurations has been elected trying to prove if this behavior appears in NACA 0012

From this moment onwards, next notation will be attributed to the different configurations:

- Unmodified wing $\left(\frac{A}{\lambda} = 0\right) \rightarrow$ **NACA 0012**
- $\frac{A}{\lambda} = \frac{0.48cm}{3.52cm} = 0.136 \rightarrow$ **NACA 0012_A**
- $\frac{A}{\lambda} = \frac{0.48cm}{1.76cm} = 0.273 \rightarrow$ **NACA 0012_B**
- $\frac{A}{\lambda} = \frac{0.24cm}{0.44cm} = 0.5455 \rightarrow$ **NACA 0012_C**

Figure 6 shows the amplitude and wavelength of a modified leading edge.

Figure 6: Tubercle dimensions [12]

2.3 Design (CATIA software)

In order to create the model, is difficult to perform the sinusoidal modification of tubercles in the leading edge. Because of that a very modern technology is used to build the model, **3D printers**, which can reach a precision of microns (in this case of 20 microns (Annexe A)). When printing a wing, first is necessary to model it in a CAD software. For this project **CATIA** is used.

As previously mentioned, this project is based in experimental aerodynamics, so a balance is needed to obtain results of forces. Is very important to take this into account because all models must be design to fit in the balance.

Usually match a specific model in this kind of scales, gives a very restricted margin, because the way of join the balance and the model required a specific component. At the end this will increase the cost and limitations of experiment. But thanks to 3D printer, this piece can be specifically created for a particular experiment. So in addition to wing model, also the joint will be design in a CAT software.

Final assembly has the following form

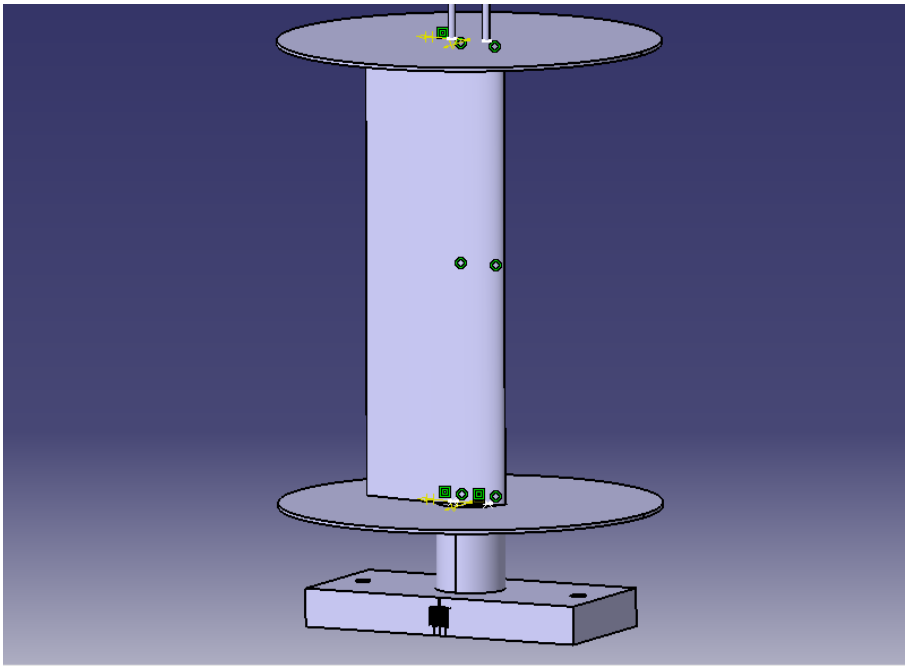

Figure 7: Final assembly

Hereunder design of all parts will be described:

2.3.1 Wing

First condition that must be keep in mind for wing design is wind tunnel dimensions. Carlos III University has at its disposal a closed wind tunnel with a test section of 0.4m x 0.4m x 1.5m (height x width x length). When choosing the span is important to take into account that the wing is divided in sections, so there must be a distance great enough between the wing and the tunnel top wall to allow the assemble of the entire wing. Finally a span of **31.2 cm** is chosen.

Selection of the chord is drive by:

- Sensibility of the scale: Initially the wing is placed with an angle of attack equals to 0^0. Experimental procedure consists on changing the angle of attack and measure the forces until stall region appears. Therefore is necessary to create a wing with a configuration such that the sensibility of the balance allows record the change in angle of attack. In

other words, if the sensibility of the scale is 0.1 N and a change in angle of attack of 3^0 produce a change in x-force of 0.07N as 0.07<0.1 this change is not going to be recorded so information is missed.

- Blockage Ratio: This effect will be described in section 6, but for now, only is necessary to take into account that as higher the chord is, worst performance will show blockage ratio. Typically, blockage ratio has values between 1% and 10%.[24]

If only sensibility of balance is consider, chord could be as high as wanted, but tunnel size and blockage will provide the upper limit restriction.

As lift coefficient for each angle of attack for NACA 0012 can be obtained from a database [25], a preliminary study to obtain the order of magnitudes of the forces that will be found, for different chord values, in the wind tunnel experiments can be made.

$$L = \frac{C_L \rho U_\infty S}{2} \tag{6}$$

- U_∞ is obtained directly measuring the velocity that will be set in the tunnel, for this experiment the tunnel is set at maximum power, reaching a velocity of 16.1 m/s.
- S correspond to the wing surface, calculating it in the XFLR5 software. Modeling the wing with its chord and span, the program gives an output of the wing surface.
- ρ assuming sea level conditions.

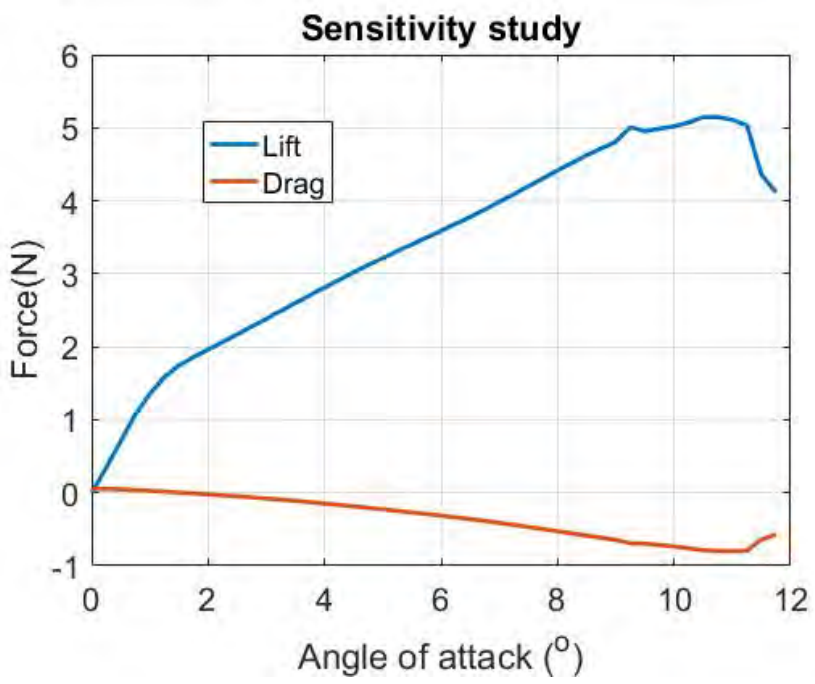

Figure 8: Forces suffer in the airfoil

Previous illustration corresponds to a wing of 8cm of chord and span of 31cm immersed in air with Reynolds number of $8.2x10^4$. Lift forces has a enough variation between angles increment to be recorded by the scale, less variation is found to be 0.1N for angles of attack near 10°. The line of drag force is not clear so it is necessary to zoom it to obtain a valid conclusion.

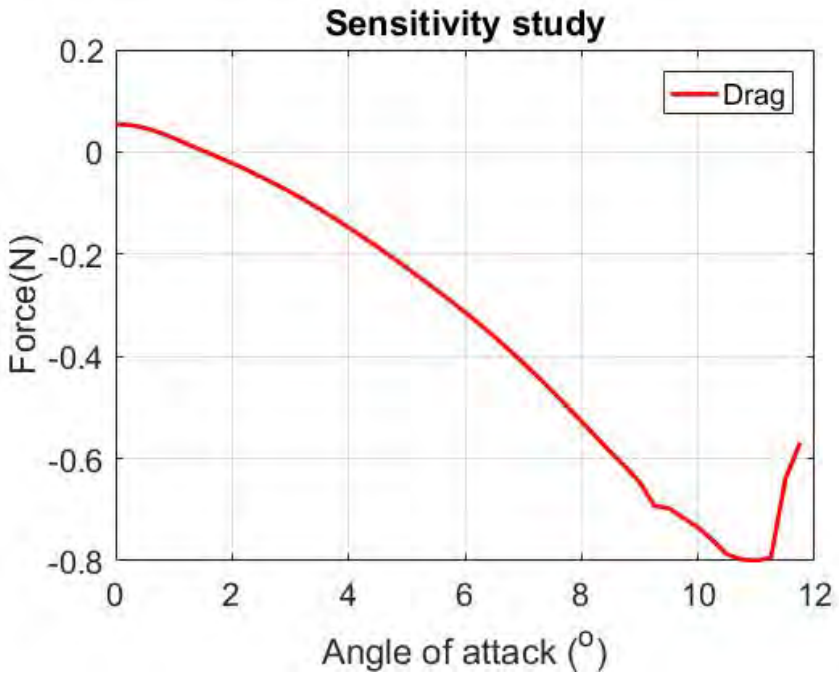

Figure 9: Forces suffer in the airfoil (Zoom)

Studying drag for scale sensibility, also fulfill the requirements. Anyway in the experimental procedure has been decided to capture data every 3°, so the margin for balance sensibility is even greater. Making the analysis of chord dimension one can notice that is not very crucial, because values of 6 cm and 7 cm are also valid.

Blockage ratio also allows clearance in the chord selection.

Finally a value for the chord of **8 cm** has been chosen.

Figure 10: Kistler balance. Image taken from [26]

Modeling a wing in CATIA can be created extruding the corresponding NACA profile over the span dimension. But for this case of study, the way of acting is different, because the chord will vary along the span due to tubercles shape, so a simple extrude action is not valid. There exist a different function for extrude a 2D section (in this case the NACA profile) which allows create a volume by extruding different sections. That means that placing different sections at different locations, CATIA can create a volume joining these sections through a given direction. Knowing that function, is possible to create a wing with tubercles. Leading edge in a modified wing will have a sinusoidal form, instead of conventional straight leading edge. Amplitude and wavelength of that sinusoid are displayed in section 2.2 which allows to know the position of peaks and valleys of the leading edge curve. Summarizing, to create a wing with leading edge tubercles, different NACA sections must be placed in peaks and valleys of the sinusoid and the sinusoid will guide the extrusion process.

First an Excel with NACA coordinates is made. The coordinates are obtained from the software XFLR5. This program allows to modify the position of the points, which is very useful in this case because for a peak an unmodified NACA will be placed while in a through, the points are changed to obtain the desired amplitude of the sinusoid.

The process to modify the point is the following:

A wing configuration is selected, for example NACA 0012_A. The amplitude wanted is 0.48 cm, so the modified NACA section, will have a chord 0.48cm smaller than the unmodified NACA. At the end, points of leading edge are displaced backward, but maintaining the value of maximum thickness, although the point where it appears change. Next figure shows different NACA sections used for the 4 configurations in XFLR5. Notice that dimensions are adimensionalized with respect to the chord.

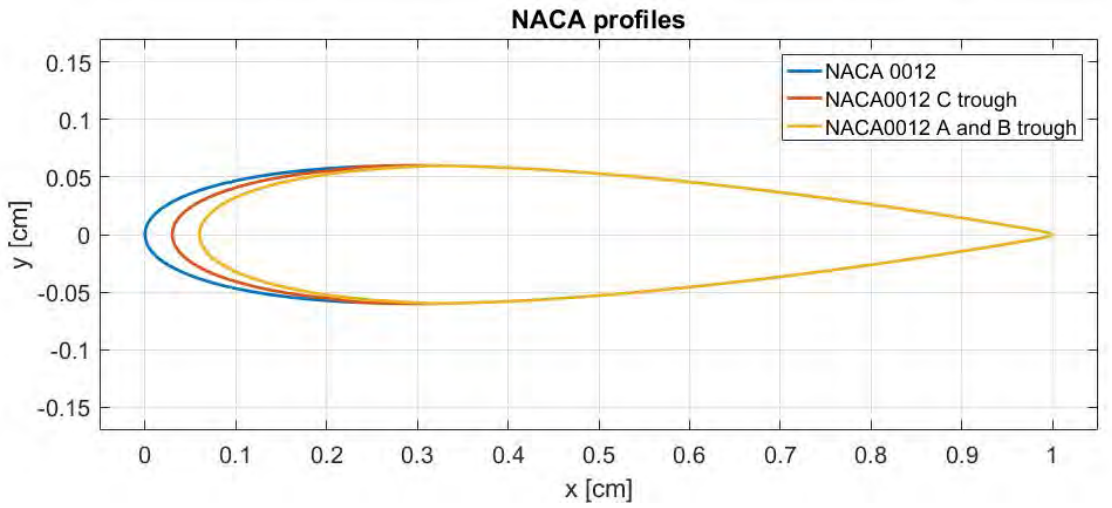

Figure 11: NACA profiles in XFLR5

Previous figure shows the dimensions and shape of the unmodified NACA (blue) and the modified profiles (red, yellow).

CATIA has the possibility of import points using an Excel macro. Coordinates x, y and z must be introduce in the macro. The units used in CATIA are meters, so the XFLR5 value should be transform to that unit. Excel macro enable to join the points imported, which will help to create de 2D NACA profile. Once the profile is imported to CATIA, a scaled must be done to reach the actual value of chord length. Remember that XFLR5 gives normalized values of chord.

To make the sinusoid guide, CATIA permits to introduce functions in the software, so inserting a sine sinusoid with the corresponding amplitude and wavelength, and applying it to a straight curve, a sinusoid is created.

$$y(x) = Asin(kx + \psi) \tag{7}$$

Previous equation is the one that governs the sinusoid form, being:

- $A \rightarrow$ Wave amplitude
- $k = \frac{2\pi}{\lambda} \rightarrow$ where λ is the wavelength
- $\psi \rightarrow$ Phase of the sinusoid. In this case a 0 phase is wanted.

To help the understanding of how modified wing is created, next illustrations show the final wing model in CATIA. First is placed an unmodified profile, blue line in Figure 11, and then a modified profile separated with a distance half of the required wavelength. Finally an extrusion following the sections is applied.

Before ending wing design, is necessary to make two holes inside the wing, for link the wing with the balance support.

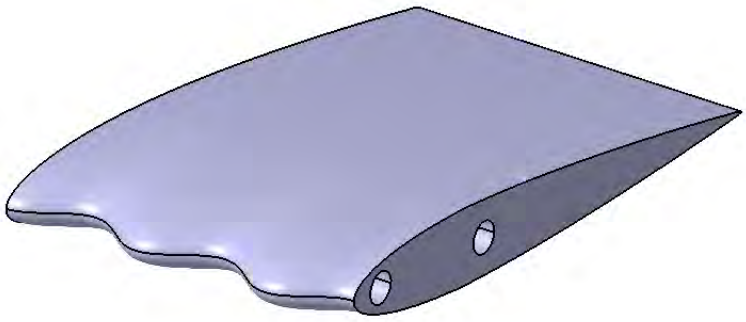

Figure 12: NACA0012_A (CATIA)

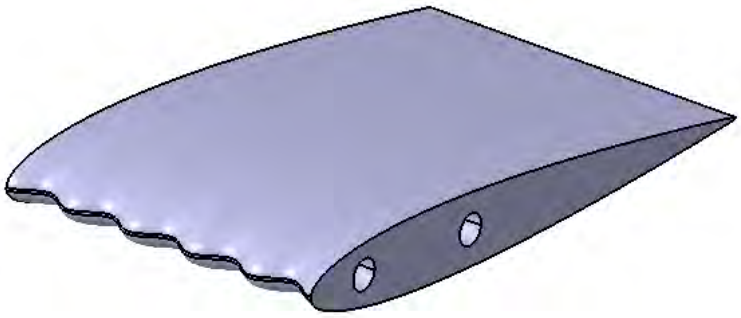

Figure 13: NACA0012_B (CATIA)

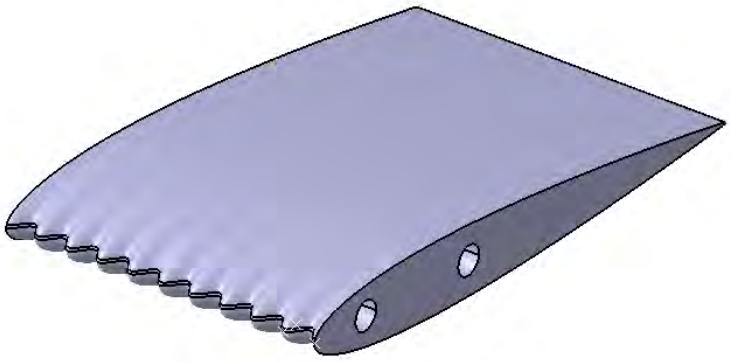

Figure 14: NACA0012_C (CATIA)

2.3.2 Balance support

Once the wing has been designed, is necessary to join it with the balance. In order to achieve that, a support is designed, divided in two parts. One devoted to place the wing in a turning surface which permit sweep along the desired angles of attack and another fixing the wing to the balance, allowing transmission of forces suffer by the wing to the balance. This last part is fixed, it does not have movable parts as the other one.

At the end a lift coefficient behavior versus angle of attack is needed, consequently several measurements for different angles of attack have to be done, being very important determine and characterized the stall region. Taking benefit of the 3D printer and its great precision (see specifications sheet in annex A) is possible to create marks with an angle spacing of 1°to be used in the experimental procedure. The cylinder is small to see an angular spacing of 1°so is decided to make grater marks every 3°and 6°. Next illustration will help to understand the model.

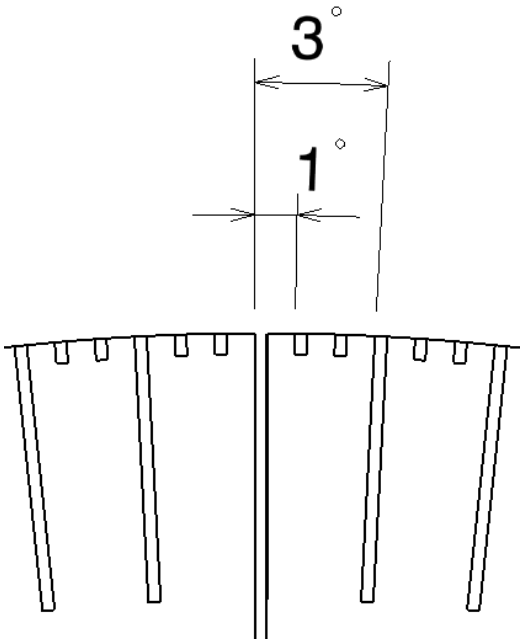

Figure 15: Angular spacing between marks

The bigger mark corresponds to the position of 0°. This is the movable part of the balance support which will have the wing fixed to it and will rotate with respect to the balance.

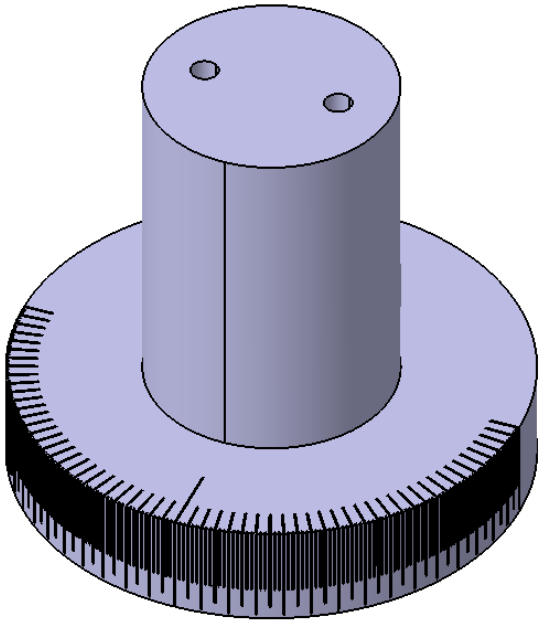

Figure 16: Movable joint

Now the fixed part of support is going to be described:

To create the union between the balance and the support, first is necessary to measure the diameters and distances of the holes in the balance where the support is connected (See Annexe B). In the support two holes are made where a screw is introduced to perform the connection between both parts.

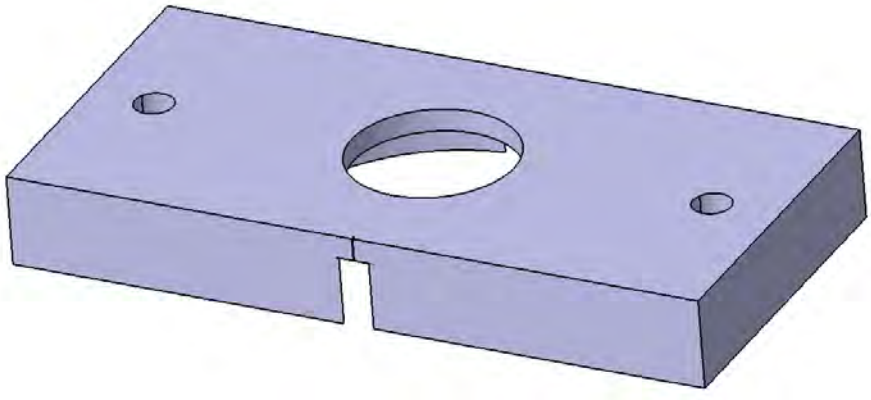

Figure 17: Fixed joint

Regarding last figure the two smaller holes correspond to the ones where the screws are introduced. The little notch helps to set the required angle easily. Finally is important to

make the holes, where the mobile part is introduced, with allowance to permit rotation between cylinders.

There exists an apparent advantage selecting this configuration. If the scale is correctly aligned with the free stream the orientation of the axes will be in wind axis. This is of benefit because is not necessary to decompose the forces. If the scale would rotate with the wing, coordinates would be body axes and in this case is necessary to decompose the forces with the angle of attack.

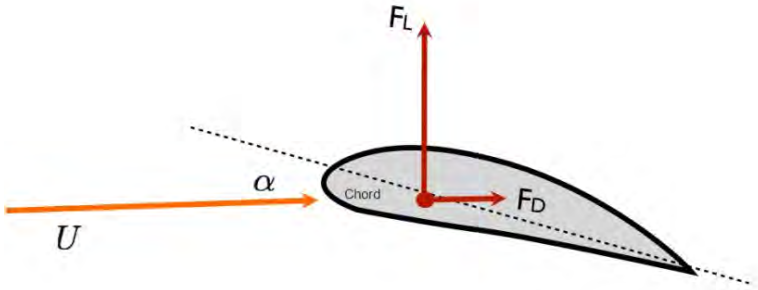

Figure 18: Airfoil using wind axis. Image taken from [27]

As can be seen, drag is always parallel to the oncoming flow. No matter the angle of attack because the direction of drag is always the mentioned before.

2.3.3 Splitter plate

Is known that a wing flying with a positive angle of attack will have less pressure at the suction side and higher pressure at the pressure side. At the tips, this difference of pressure will produce that the flow of the pressure side goes to the upper side of the wing producing a winding of the flow which ends in tip vortices. In the tips the lift will be equals 0 because the flows of upper and lower side will mix. This effect, together with the fact that in the suction side the flow moves slightly to the root and in the pressure side the flow moves slightly to the tip, will produce a pressure gradient along the spanwise direction. To avoid it, is necessary to place a flat plate in the wing tips. With the plate is achieved that the pressure gradient in the span direction is produced only by the tubercles. [28][29]

Another aim of putting plates, is reduce the interaction of the boundary layer produce by the tunnel walls. [30]

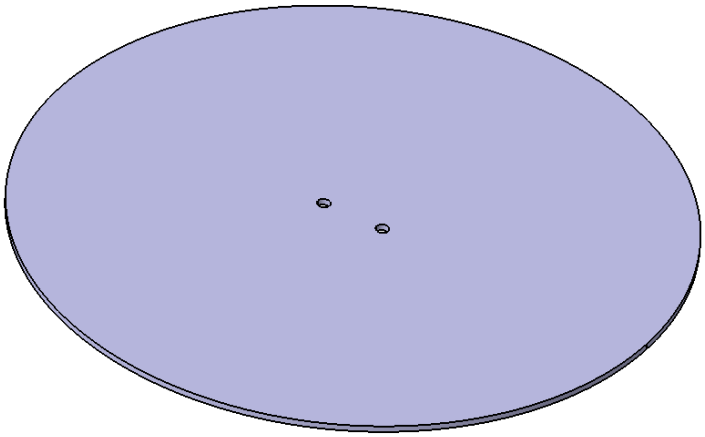

Figure 19: Splitter plate

Note that holes are design in a way that the axis of rotation of the support lies in the quarter chord of the wing (c/4) which corresponds to the aerodynamic center in subsonic flow, point where moment coefficient becomes independent on angle of attack.

2.4 Model assembly

Once all the pieces are mounted it should be assembled as in Figure 7. Before, all parts printed with the dust printer should be sanded to get a smoother surface.

The wings have the following form:

- NACA 0012

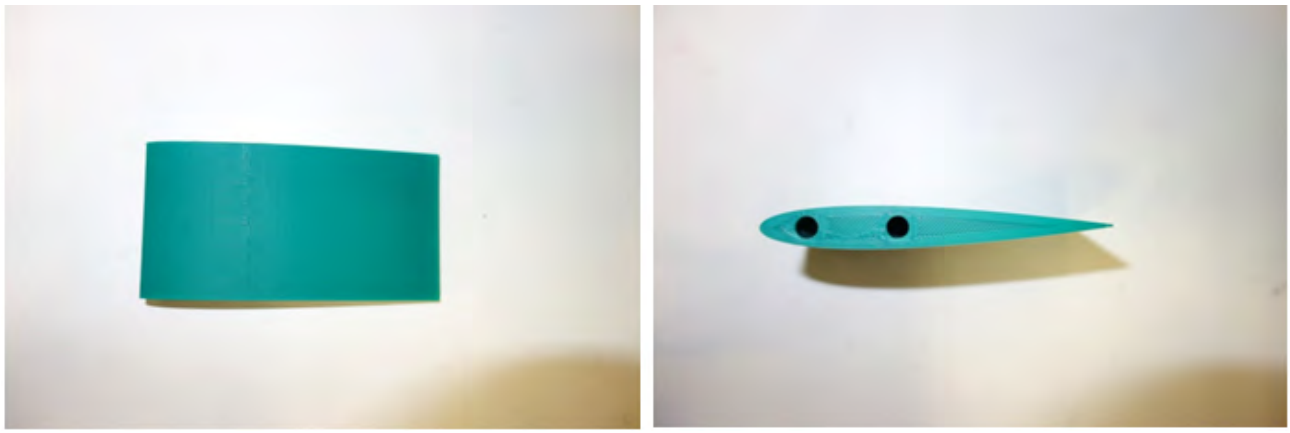

Figure 20: NACA 0012

- NACA 0012_A

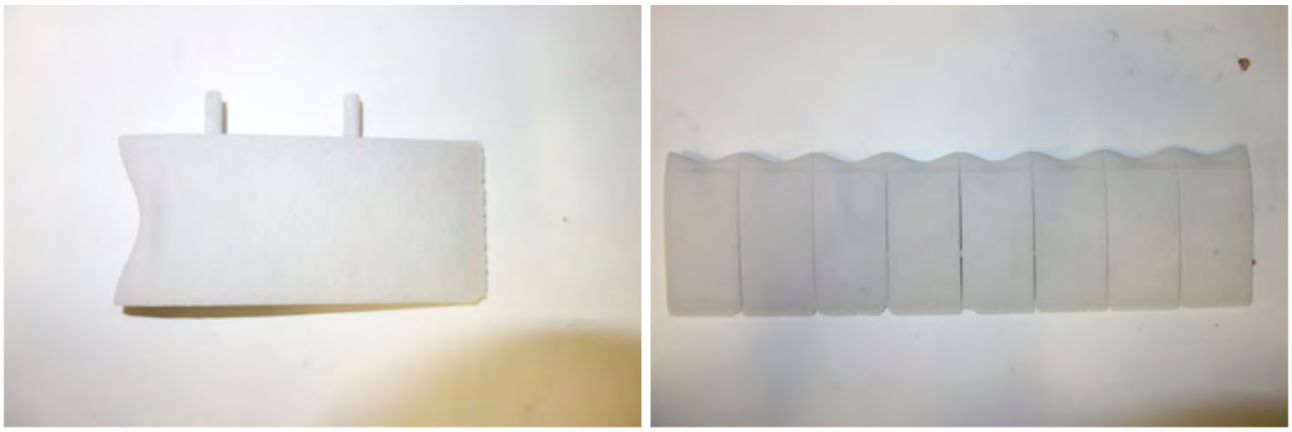

Figure 21: NACA 0012_A

- NACA 0012_B

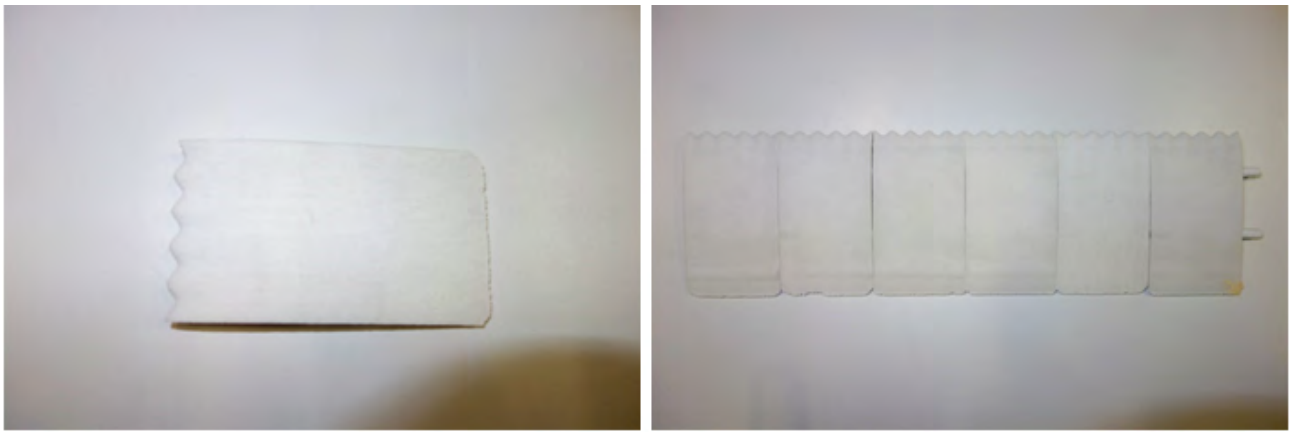

Figure 22: NACA 0012_B

- NACA 0012_C

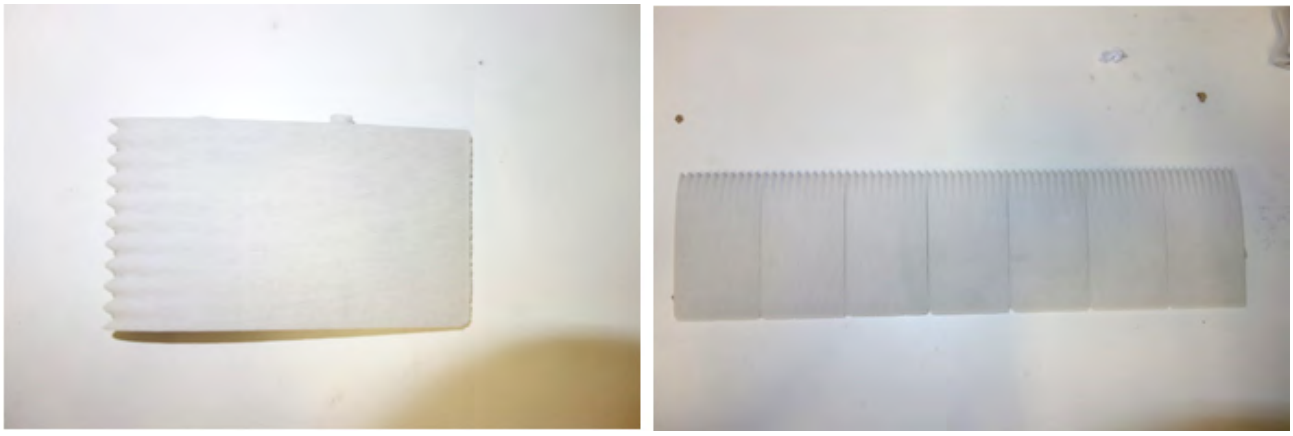

Figure 23: NACA 0012_C

In Figure 20, a pair of holes can be seen. In the same way it appears in the plate and in the profiles of all wings. Inside that holes, two rods are introduce in order to hold all the parts together. The assembly without the wing can be seen in next figure:

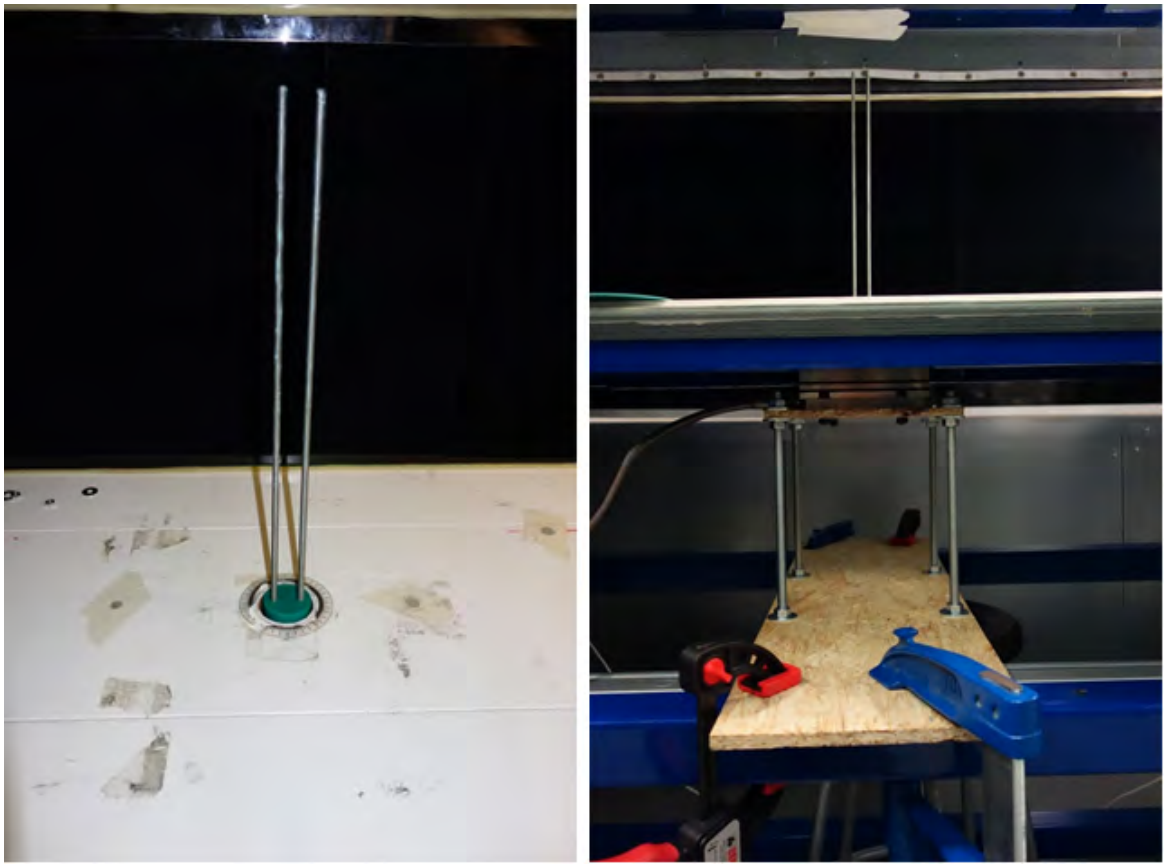

Figure 24: Assembly without wing

In the image on the left, the cylinder is observed at the bottom of the rods, the cylinder is not in contact with the walls, this is very important because if it touches the walls, some force will be transmitted to the walls and the scale will record error information.

When adding the wing, is necessary to put the circular plate to avoid three dimensional effects as explained in section 2.3.3

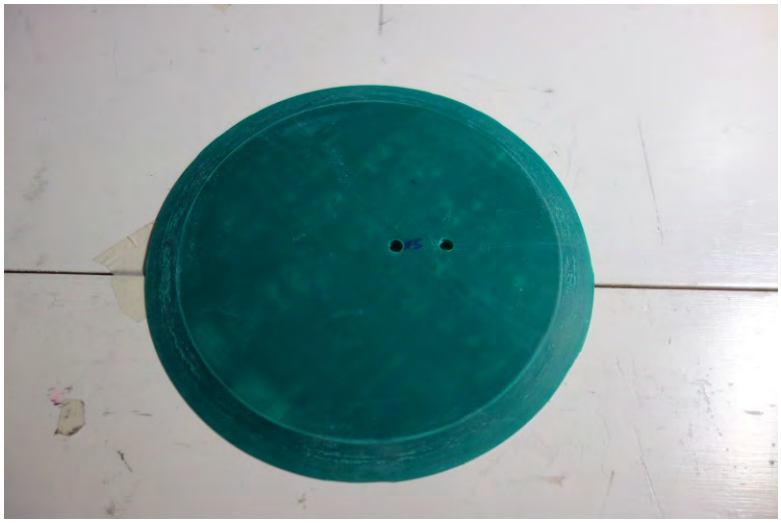

Figure 25: Circular plate

Being finally the assembly:

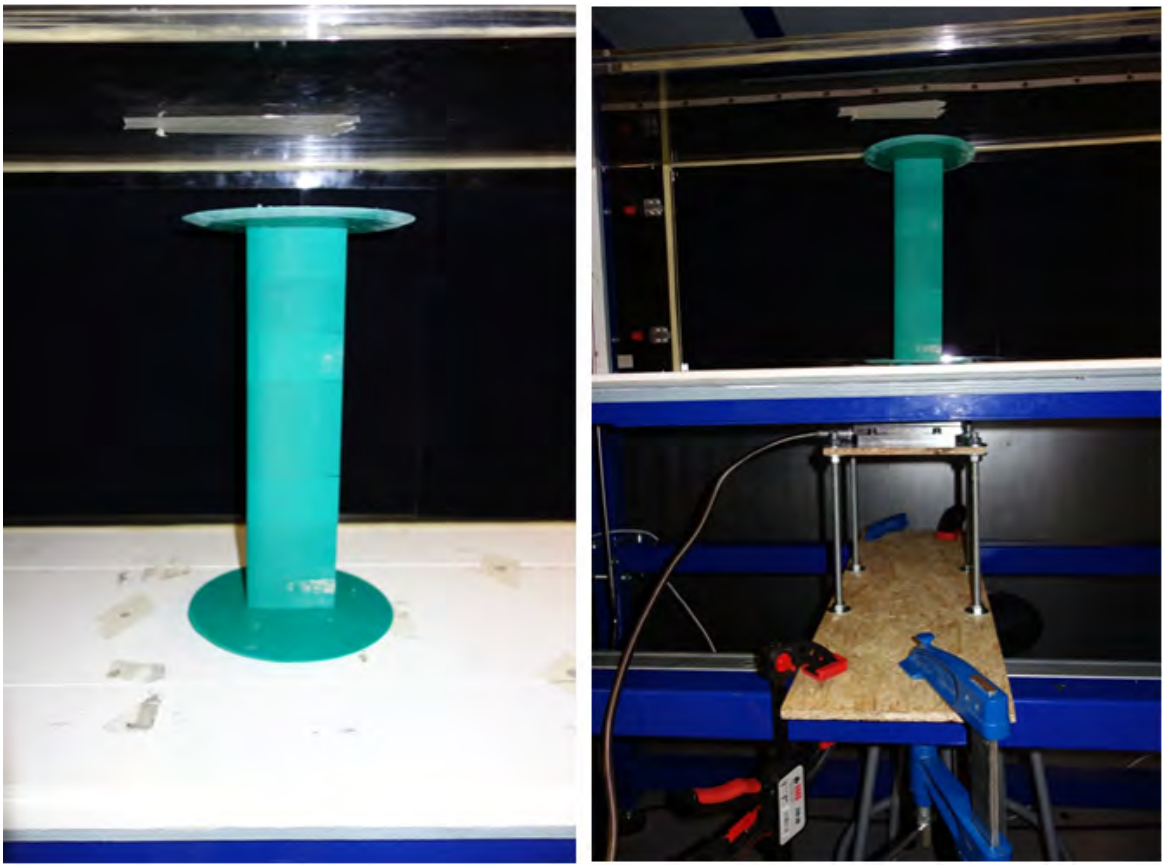

Figure 26: Final assembly

2.5 Data acquisition

When all is ready for the experiment the test section is closed with a methacrylate screen. Then two measurements are made at each angle of attack, the first one starting at 0 m/s velocity and accelerating to maximum power and the second measurement with the tunnel at maximum power during all the measurement.

With the first measurement the tare of the scale is obtained, because when it should record 0 value of force, it reads a little value different than 0 and it must be taken into account.

The scale sends electrical signals to the Data Acquisition System but this signal is in mV and it need to be amplified to a range of potential that can be read by the scale so an amplifier is needed.

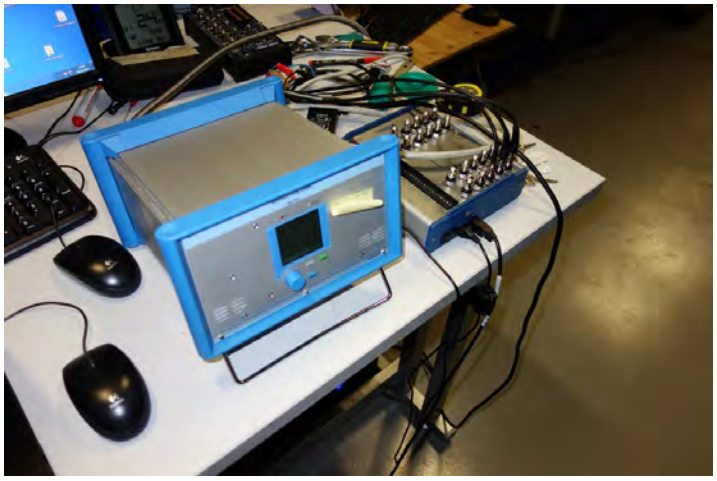

Figure 27: Amplifier

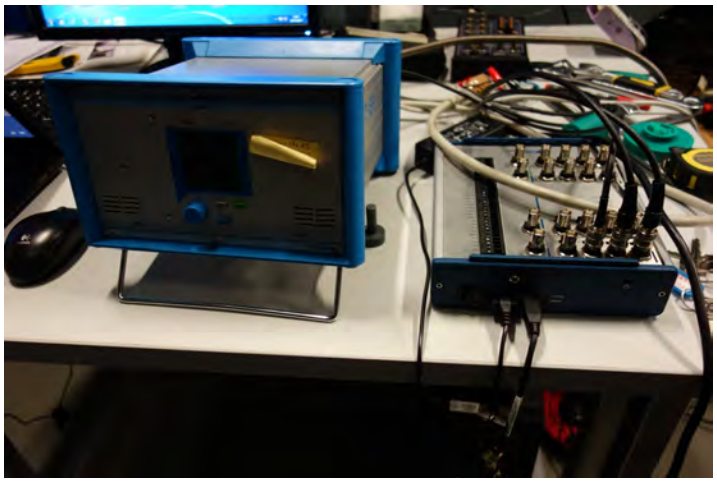

Figure 28: Amplifier (left) & Data Acquisition System (right)

3 Reynolds Number Influence

Reynolds number is a dimensionless quantity that relates the ratio of inertial forces to viscous forces. Inertial forces are characterized by density, velocity and gradient of velocity, while the viscous forces are governed by dynamic viscosity and second gradient of velocity. [31]

$$Re = \frac{\rho\, v\, dV/dx}{\mu\, d^2V/dx^2} \tag{8}$$

Velocity gradient is proportional to V/L and second gradient proportional to V/L^2 ,obtaining finally:

$$Re = \frac{\rho\, v\, V/L}{\mu\, V/L^2} = \frac{\rho\, V\, L}{\mu} \tag{9}$$

Depending on the value of Reynolds number, flow can be laminar or turbulent:

- Laminar flow appears for low Reynolds number and is characterized by domination of viscous forces. If velocity is smaller, viscous forces has a greater influence.
- Turbulent flow takes place for high values of Reynolds, dominated by inertial forces and the appearance of vortices and eddies.

When increasing Reynolds number and reaching the limit between laminar a turbulent (critical Reynolds number) the change in flow behavior is not instantaneous, so a new regime appears, called **laminar-turbulent transition**. This regime is still complicated to determine and study its influence because is a midway between laminar and turbulent, appearing influences of the two regimes.

As mentioned before in the experimental set up section, Reynolds number can be considered low, which has some effects in the profile. Low Reynolds number has a very important effect in separation. Profiles flying in small values of Reynolds number will lead to Laminar Separation Bubble. According to [32] Laminar Separation Bubble will be found in wings flying in a Reynolds range between 10^4 and 10^6. As Reynolds values increases, the length of the separation bubble decreases until a point where the value is high enough to bubble separations disappears and another type of stall takes place. Bubble separation is not only influenced by Re, also angle of attack has a high influence, it has sense because stall occurs when angle of attack is high and the adverse pressure gradient cause a loss of lift. Greater angles of attack move the laminar separation point towards the leading edge without changing the length of the bubble. There exist a value of angle of attack that will produce a big adverse pressure gradient, breaking the bubble and producing a catastrophic drop in the lift value (stall). The type of stall is appropriate for this experiment because the abrupt drop in lift must be softened by the tubercles.

Next image will help to understand the flow pattern. Free stream flow is attached to the surface but due to viscous forces a laminar separation appears, creating a separation bubble (shown in the image as stagnation air and reverse flow). Note that behind the reverse flow the

airflow again attaches to the surface because the momentum transfer due to the turbulent zone, eliminate the reverse flow zone. [33]

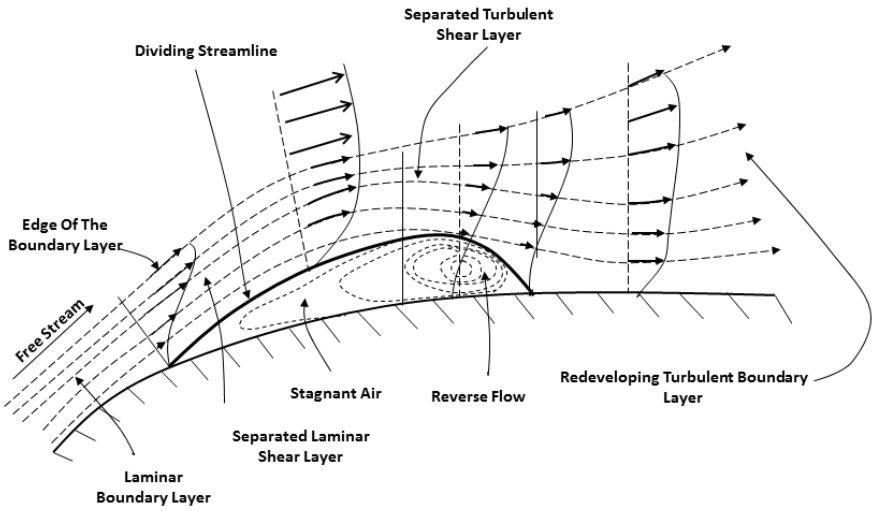

Figure 29: Flow pattern in laminar separation bubble. Image taken from [33]

4 Printing process

Initially all models would be printed in plastic. Plastic 3D printers operates melting the plastic and constructing layer by layer the require shape. The problem is the contraction of the material when plastic cools. To avoid that, the wing is divided into several sections and then all of them will be joined. Still the contraction of material affects the geometry so finally was decided to change the 3D printer and use a dust printer to avoid that problem. Dust printer has a resolution of 89 microns [34]. For the rest of the parts as the support and plates, plastic printer is used. The material used is ABS plastic, characterized by its rigidity, tenacity and hardness.

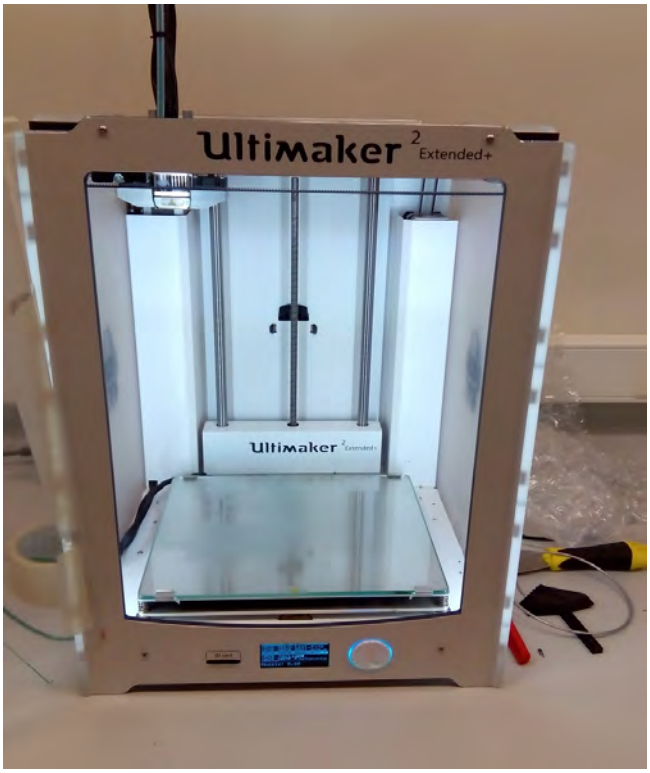

Figure 30: Ultimaker 2 Extended+ (Plastic 3D printer)

Figure 31: ZPrinter 450 (Dust printer)

5 Validation

When performing an experimental analysis is necessary to validate the experiment. The way to proceed consists on compare the results obtained with a data base, a previous certified experiment or a simulated data obtained with software.

Software XLFR5 is used to achieve a validation of the model.

XLFR5 was not created for professional use, for this reason it cannot be declared as a flawless program. However XFLR5 has been hardly tested, comparing with other softwares obtaining an important degree of success. Thus is possible to ensure that the results acquired with the software are enough reliable.

Remember that performing the experimental procedure, two plates were placing in order to avoid three dimensional effects, so the analysis set in the simulation program will be a 2D analysis. XFLR5 incorporate a database of NACA arifoils, so NACA 0012 is created. Once the section profile is determined, is time to create an analysis. XFLR5 defines operational points (OpPoint) which are defined by its angle of attack and Reynolds number, always associated to a profile and a polar. Every time that convergence in the analysis is reached, an operational point is created and the data is stored in a polar [35]. To validate, the same value of Reynolds number as the wind tunnel is set, Re=8.2x10^4 and a range of angles of attack 0°to 15°

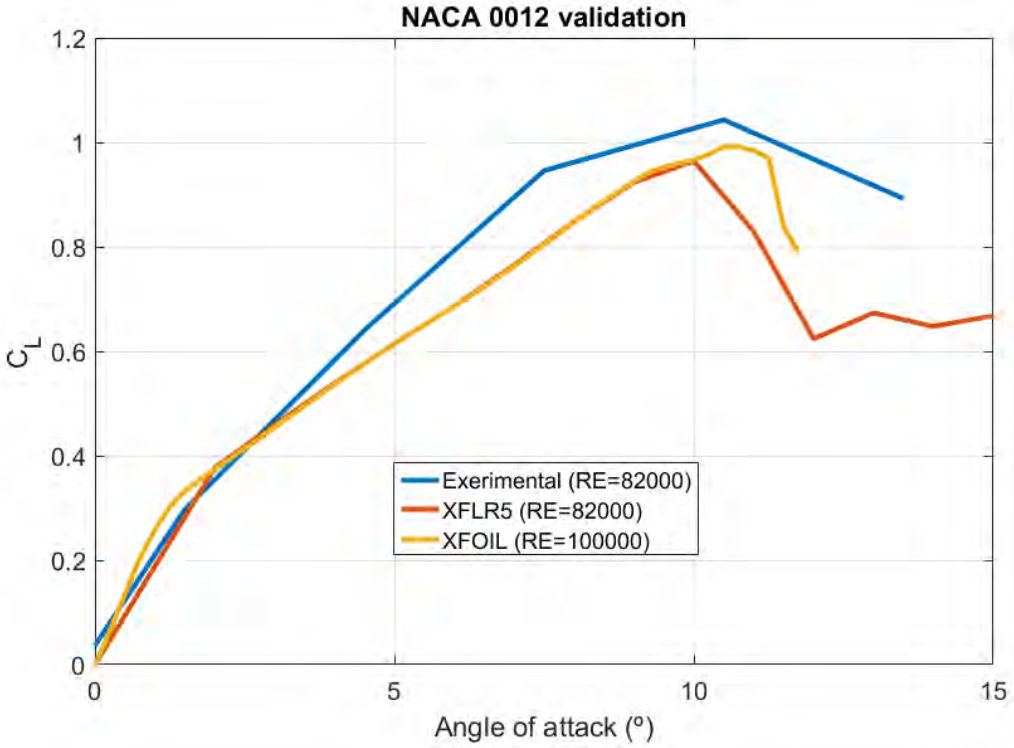

Figure 32: Experimental data validation

As can be seen in the previous figure, there exist a very good agreement between the experimental and numerical data obtained in XFLR5. The experimental line does not cut the zero value because is impossible to obtain a perfect 0 value of lift due to errors in the printing process, errors in the scale, measurements errors. However the value is very close to 0. The stall region appears, more or less, at the same angle of attack $\approx 10°$, but in the experimental data it seems to be less catastrophic. It can be produce by the vibration of the wing when stall appears. In the solutions obtained from XFLR5 the stall produces a more pronounced loss of lift.

Another way of validating the model is search databases on Internet, for example in the Airfoil tools database uses XFOIL software (similar to XFLR5). In the graph can be seen also the comparison between the experimental data at Re=$8.2 \text{x} 10^4$ and the airfoil tolls results at Re=$1 \text{x} 10^5$, obtaining again a good agreement between both curves.

It is important to notice that the lift coefficient slope is not perfectly linear, in both figures appears a change in slope approximately at 3°, this is caused by the low Reynolds number value. Stall point and values of C_L are once more time very similar. Also note the perfect agreement between XFLR5 and XFOIL. In prestall region, this behavior is expected because the only variable changed for varying the Reynolds number, is the velocity and the slope should be the same. However the stall region differs because these kinds of softwares have problems when characterizing stall region. It sees a region where a loss of lift appears but does not characterized the stall region as in reality.

At the end can be determined that the experimental model is validated.

6 Wind tunnel corrections

Wind tunnels provide one of the best recreation of the behavior of a body immersed in a fluid environment. A small summary of main wind tunnels characteristics is made to get an overview of how it works.

The body to be analyzed is introduced in the test section, so the flow must be adapted to obtain the require flow conditions. The flow must has the greatest velocity at this test section so using mass conservation principle, making a smaller area in the test section that in the other parts, the maximum velocity is achieved. That means that before the test section a contraction zone must appears and after test section an expansion zone must be placed.

$$\rho_1 A_1 V_1 = \rho_2 A_2 V_2 \tag{10}$$

Assuming constant density, a reduction in area will cause an increase in velocity.

Once the flow acceleration is accomplish, it is very important to create a uniform free stream. The settling chamber is the part assigned to that task. In order to fulfill the specifications, screens and honeycomb are used. Rotating blades produces the necessary flow velocity but at the same time the free stream converts in a rotating airflow caused by the fan, to avoid that problem screens are used, which is a kind of mesh, breaking the rotating behavior of the airflow. Uniform flow is another concern when adapting the flow. Placing honeycomb before test section is possible to reduce considerably lateral velocity which will induce wrong results. [36]

Reynolds number is crucial for reproducing flight conditions.

$$Re = \frac{\rho U_\infty c}{\mu} \rightarrow Assuming\ \ ideal\ \ gas \rightarrow \rho = \frac{p}{RT} \rightarrow Re = \frac{\rho U_\infty c}{\mu RT} \tag{11}$$

Large commercial aircrafts flight at Reynolds of order of magnitude $3x10^7$ [37]. Regarding previous equation can be notice that to obtain a large Reynolds number is necessary to have a big model (big c). Additionally there exist other possibilities to increases that value, increasing the pressure or decreasing temperature and gas constant (R). University has at its disposal a subsonic closed wind tunnel where the tests are made.

However experiments in tunnels do not reproduce totally the reality, consequently is necessary to introduce some corrections. Main cause of dissimilarity, is the fact that in real flight the test section area can be considered as infinite and the wake can grow without boundaries.

- Horizontal Buoyancy: This effect is caused by the variation of static pressure along the test section when no model is present inside the section. The normal actuation should be a constant static pressure along all the test section, but this is not possible because flow velocity is not perfectly constant and direction is not perfectly straight. Consider negligible in this experiment.

- Solid Blockage: In real operations the ratio of frontal area and stream cross sectional area is 0, because as said before the section area of free stream is infinite. But in wind tunnels that ratio is different from 0, being typically 0.05. This result in a higher surface stresses due to the change in oncoming flow or dynamic pressure.
- Wake blockage: Due to the closed test section, the wake cannot grow totally. As higher is the wake the correction should be also greater. Notice that in an open closed test section this effect is negligible because the wake can expand as much as possible. Wake blockage produce an increase in drag.
- Streamlines curvature: Due to finite distances to boundaries the streamlines will suffer an alteration on its curvature, ending in higher values of lift, drag and moment in comparison with the real case. At the walls of the test section separation can occurs affecting stream lines and flow characteristics. Consider negligible in this experiment.
- Normal downwash change: Refers to the component of induced flow in the lift direction at the test article. In a closed test section lift is greater so for a given angle of attack, a smaller downwash will appears than in an unbounded case. For an open jet, opposite effect takes place. Consider negligible in this experiment.

6.1 Solid Blockage

The presence of tunnel walls reduce the area where the flow pass through, ending in flow acceleration according to continuity equation. This acceleration, which is approximated constant, because it cannot occur instantaneously, is called solid blockage. Solid blockage depends on thickness, thickness distribution, and model size. Velocity increment at the model is much less than the velocity increment in the area reduction zone, about one fourth.

Following formula is obtained from [38], where a body is modeled as a distribution of sources and sinks, contained in the tunnel walls, modeled by infinite distribution of images.

$$\epsilon_{SB,W} = \frac{k_1 \tau_1 V}{C^{3/2}} \tag{12}$$

- K_1 is the body shape factor and can be obtained from Figure 33. Wing geometry gives a thickness ratio of t/c=0.12. NACA 0012 profile corresponds to an airfoil series of 4 digits. So the value for the body shape factor is:

$$K_1 = 1.01$$

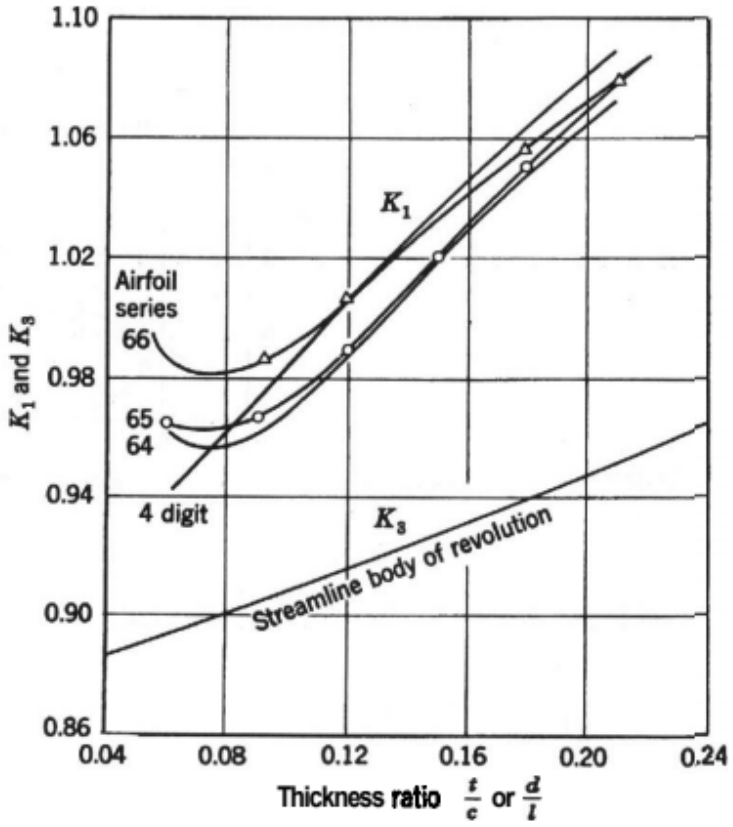

Figure 33: Body shape factor. Image taken from [24]

- τ_1 can be calculated with Figure34. Tunnel dimensions are breadth (B) of 0.4m and height (H) of 0.4 m. For the dimensions of the tunnel used those values are 0.4m so the ratio $\frac{B}{H} = 1$. Then the relation between wing geometry and tunnel size is establish as $\frac{2b}{B}$, but for this case is $\frac{b}{B} = \frac{0.3231}{0.4} = 0.807525 \rightarrow \tau_1 = 0.885$

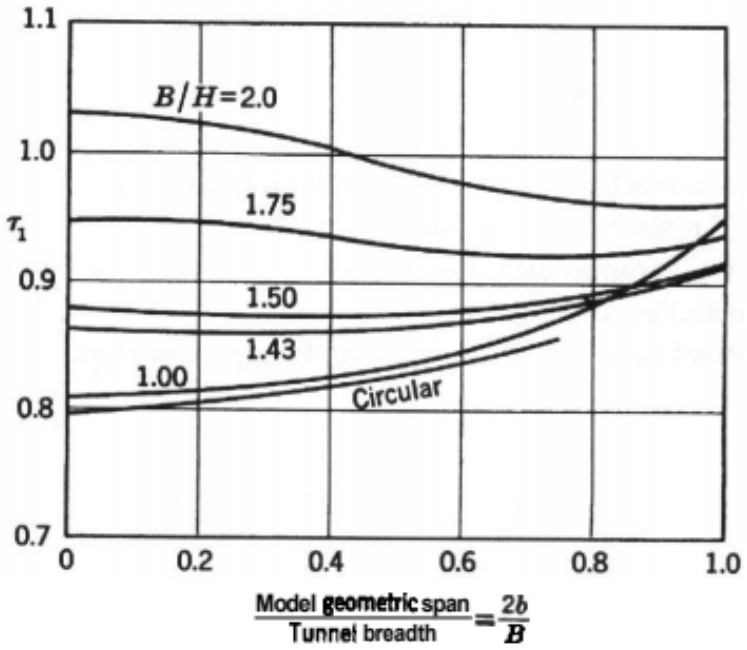

Figure 34: Body shape factor. Image taken from [24]

- V refers to the wing volume and there are two ways of calculating it. Obtaining the cross sectional area of the profile and multiplying by the span, or creating the wing model in XFLR5 software and directly it gives the wing volume. Note that the wing with the greatest volume is the unmodified because the leading edge has no modifications.
- C correspond to tunnel test section area: $B \cdot H = 0.4 \cdot 0.4 = 0.16m^2$

$$\epsilon_{SB,W} = \frac{1.01 \cdot 0.85 \cdot 0.00017m^3}{(0.16m^2)^{3/2}} = 0.00237 \tag{13}$$

6.2 Wake blockage

According to [39], when separation occurs is necessary to consider momentum effects outside the wake. The presence of wall boundaries in the tunnel, results in a lower wake pressure and lower base pressures than in free air conditions. Equating momentum conservation:

$$D + p_b B = \iint_C (p_1 + \rho u_1^2) dydz - \iint_{C-B} (p_2 + \rho u_2^2) dydz \tag{14}$$

1 correspond to the plane of incoming flow and 2 the plane of out coming flow in the test section tunnel. D correspond to the total drag, C cross-sectional area and B the cross-sectional area of the effective wake at the exit plane 2. Equation (14), shows the influence outside the

wake $(C - B)$ in the momentum equation. Developing momentum equation with Bernoulli's equation:

$$p_1 + \frac{1}{2}\rho(u_1^2 + v_1^2 + w_1^2) = p_2 + \frac{1}{2}\rho(u_2^2 + v_2^2 + w_2^2) = P + \frac{1}{2}\rho U^2 \tag{15}$$

Assuming lateral velocities very small in comparison with forward velocity, terms v and w can be neglected. At the end the following expression is obtained:

$$\epsilon_{wb,f} = \frac{S}{4C}C_{D0} + \frac{5S}{4C}(C_{Du} - C_{Di} - C_{D0} \tag{16}$$

Note that for unseparated flow $C_{Du} = C_{Di} + C_{D0}$ so the second term in Equation (16) vanishes.

Solid blockage and wake blockage is different for each wing configuration because the term C_{D0} correspond to the drag at 0 angle of attack and it is different for each wing

The total blockage is:

$$\epsilon_T = \epsilon_{sb,W} + \epsilon_{wb,f} \tag{17}$$

The final effect in the wing is a change in the dynamic pressure, so lift and drag is influenced by blockage.

$$q_C = q_A(1 + \epsilon_T)^2 \tag{18}$$

All the information developed in this section has been obtained from [24]

The values of blockage obtained for each wing are:

Case	Blockage ratio
NACA 0012	0.0318
NACA 0012_A	0.0162
NACA 0012_B	0.0332
NACA 0012_C	0.0423

Table 1: Blockage ratio

As can be seen the values are between 0.01 and 0.1 as stated in [24]. Is expected that values because there are not a great difference between them.

7 Uncertainty calculation

In all experimental studies, errors appear due to measurement instruments, and it must be quantify. The unique situation when the error can be determined entirely occurs in calibration because in this situation the exact value expected from the instrument is known. That is the reason why the term uncertainty is used, because it refers to a possible value that error might have. A variable with its uncertainty is expressed as:

$$X_i = X_i\,(measured) \pm \delta X_i \tag{19}$$

Following the Root-Sum-Square (RSS) is possible to know the uncertainty of the result of the experiment R by its variables X_i:

$$\delta R_{X_i} = \frac{\partial R_{X_i}}{\partial X_i}\delta X_i \tag{20}$$

The first term in the equation is called the sensitivity coefficient and establishes how the result varies with the variable studying. Second terms stands for the uncertainty of the variable. Applying the RSS to this experiment is necessary to establish the uncertainty of the lift and drag coefficients.[40]

Lift coefficient depends on Lift, speed, density and wing surface. There are more than one variable, so to obtain the total uncertainty the root sum square must be performed.

$$\delta R_{X_i} = \left\{ \sum_{i=1}^{N} \left(\frac{\partial R_{X_i}}{\partial X_i}\delta X_i \right)^2 \right\}^{1/2} \tag{21}$$

The uncertainty term of each variable is determined by:

- $\delta L \rightarrow$ Lift is obtained from the scale which gives as an output an electric signal. The uncertainty of that signal is obtained applying the standard deviation which quantifies the amount of variation or dispersion of a set of data values. If the data points are farther from the mean value, the deviation will be higher [41]. Standard deviation is easily computed with the Matlab function *"std"*.
- $\delta U_\infty \rightarrow$ Uncertainty of wind tunnel velocity is estimated to be 0.2 m/s. Measured with a pitot-tube.
- $\delta \rho \rightarrow$ Assuming an uncertainty of 5% in ρ measurement, the density uncertainty yields $1.225 \cdot 0.05 = 0.06125 kg/m^3$. This uncertainty is caused by the variation of temperature in the tunnel after many time measuring.
- $\delta S \rightarrow$The uncertainty of surface comes from the uncertainty of the ruler, which is half of the smaller distance measurable with the ruler: $1mm/2 = 0.5mm$. A surface is being determine so it must have dimensions of mm^2 $0.5mm \cdot 0.5mm = 0.25mm^2$
- $\delta \alpha \rightarrow$ As the angular separation of the cylinder marks are 1°the uncertainty is the half of it: 0.5°

Note that for each measurement the unique value that changes is the lift, so the uncertainties of velocity, density and surface remain constant. For the Lift coefficient uncertainty, it must be derived with respect velocity, surface, density and lift, obtaining a final expression for the uncertainty:

$$\delta C_L = \left(\left(\frac{\delta L}{0.5\rho S U_\infty^2} \right)^2 + \left(\frac{-4L\,\delta U}{\rho S U_\infty^3} \right)^2 + \left(\frac{-2L\,\delta \rho}{\rho^2 S U_\infty^2} \right)^2 + \left(\frac{-2L\,\delta S}{\rho S^2 U_\infty^2} \right)^2 \right)^{1/2} \tag{22}$$

$$C_L = C_L\,(measured) \pm \delta C_L \tag{23}$$

To express in percentage the error:

$$\epsilon = \left(1 - \frac{C_L + \delta C_L}{C_L} \right) \cdot 100 \tag{24}$$

For the Drag coefficient same procedure must be followed but using the data obtained from the scale determining the drag instead of the lift.

To summarize the uncertainties, a table displaying the maximum uncertainties for each variable and measurements is shown.

Case	Variable	Uncertainty
NACA 0012	C_L	± 0.65%
	C_D	± 1.3%
	C_L/C_D	± 2.44 %
NACA 0012_A	C_L	± 1.4%
	C_D	± 0.95%
	C_L/C_D	±2.82%
NACA 0012_B	C_L	±0.92%
	C_D	±0.77%
	C_L/C_D	±2.8%
NACA 0012_C	C_L	±2.69%
	C_D	±0.64%
	C_L/C_D	±2.46%

Table 2: Uncertainties

8 Results

Before this point, the problem has been presented and exposed, including the preparation, corrections and measurement process. Now is time to present, discuss and compare the results obtained.

First the four main aerodynamics characteristics of each NACA will be shown, Lift coefficient, Drag coefficient, Polar and aerodynamic efficiency. Then comparison between the four models will be done trying to determine see if the target of smoothing stall region is achieved.

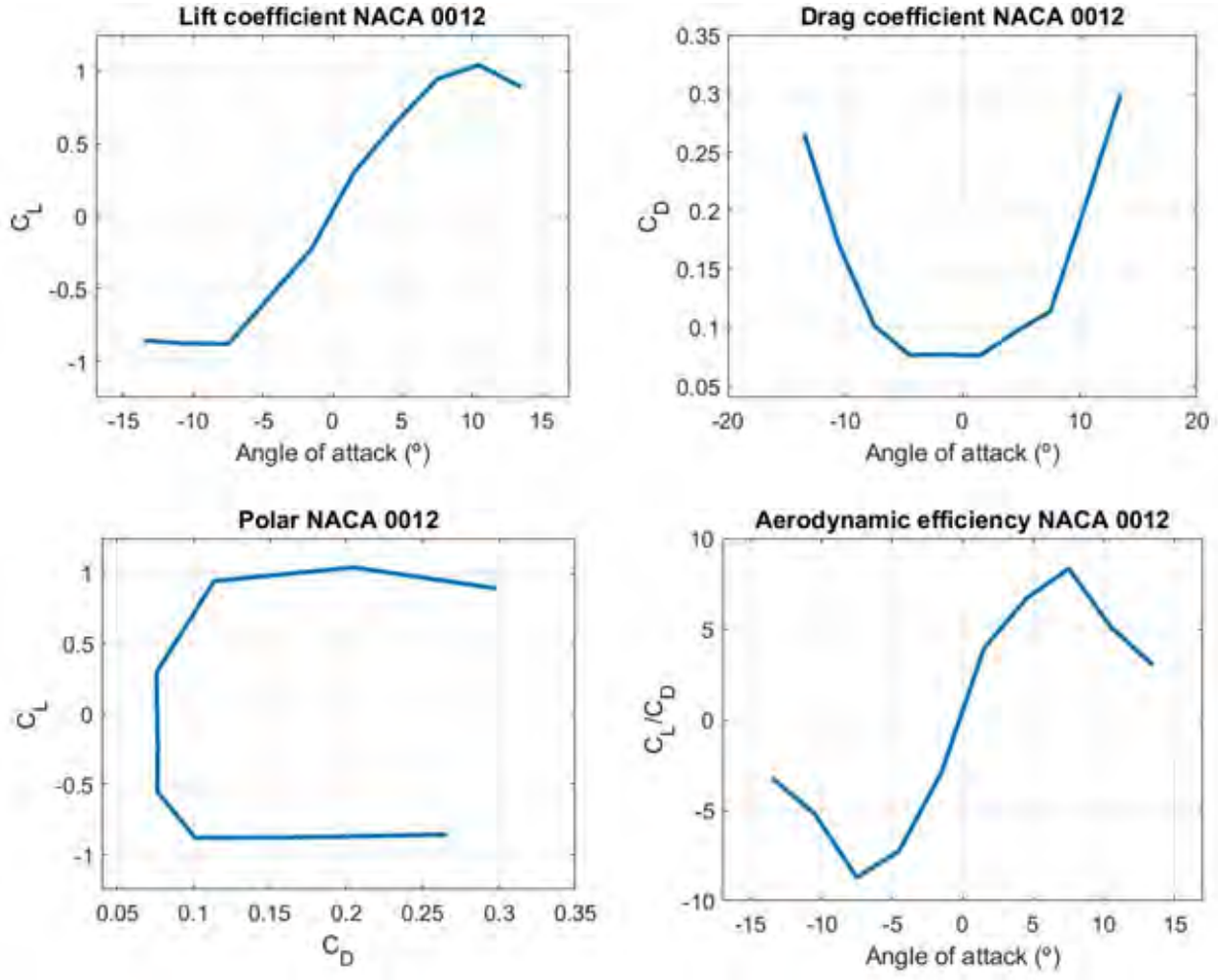

Figure 35: Results NACA 0012

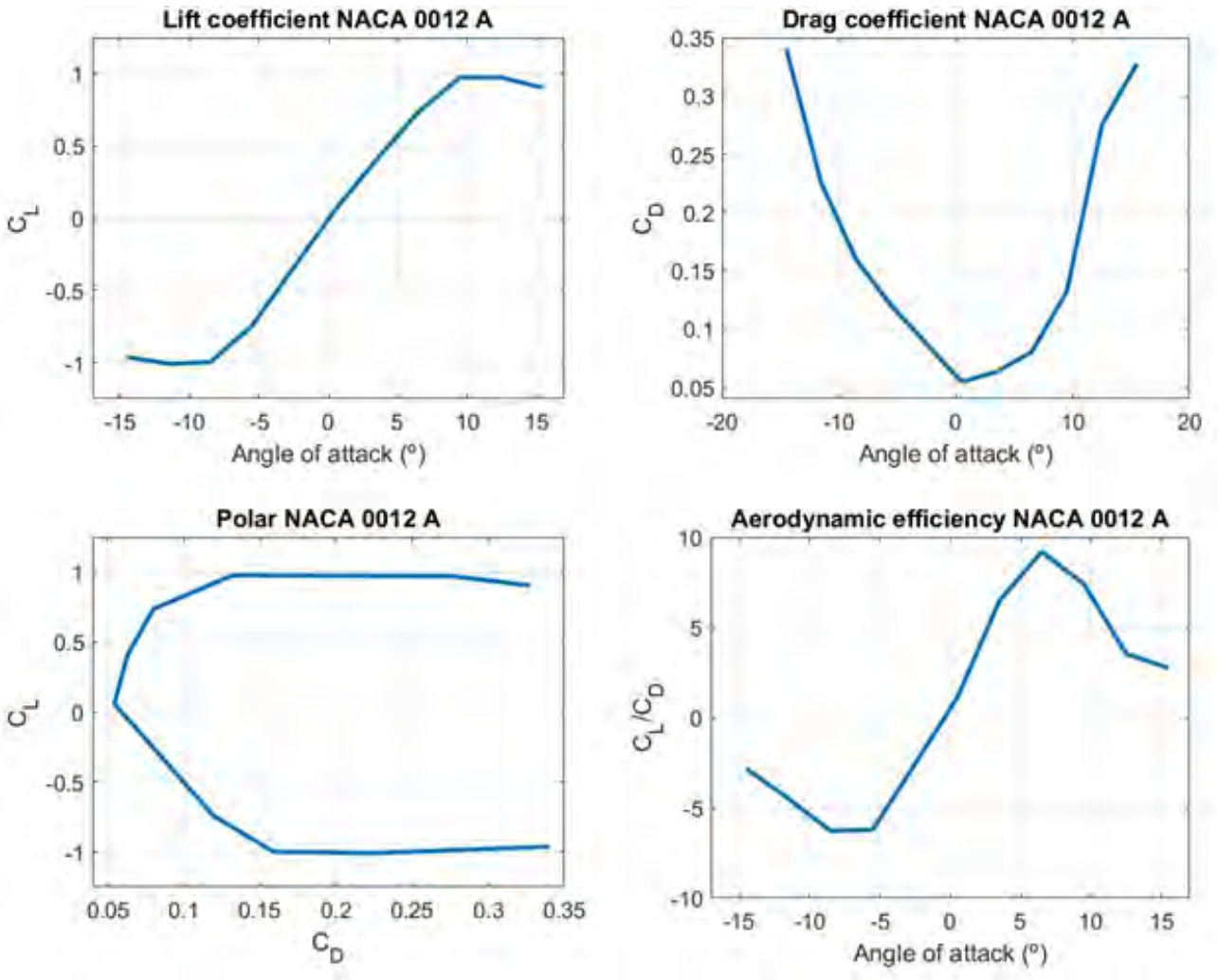

Figure 36: Results NACA 0012_A

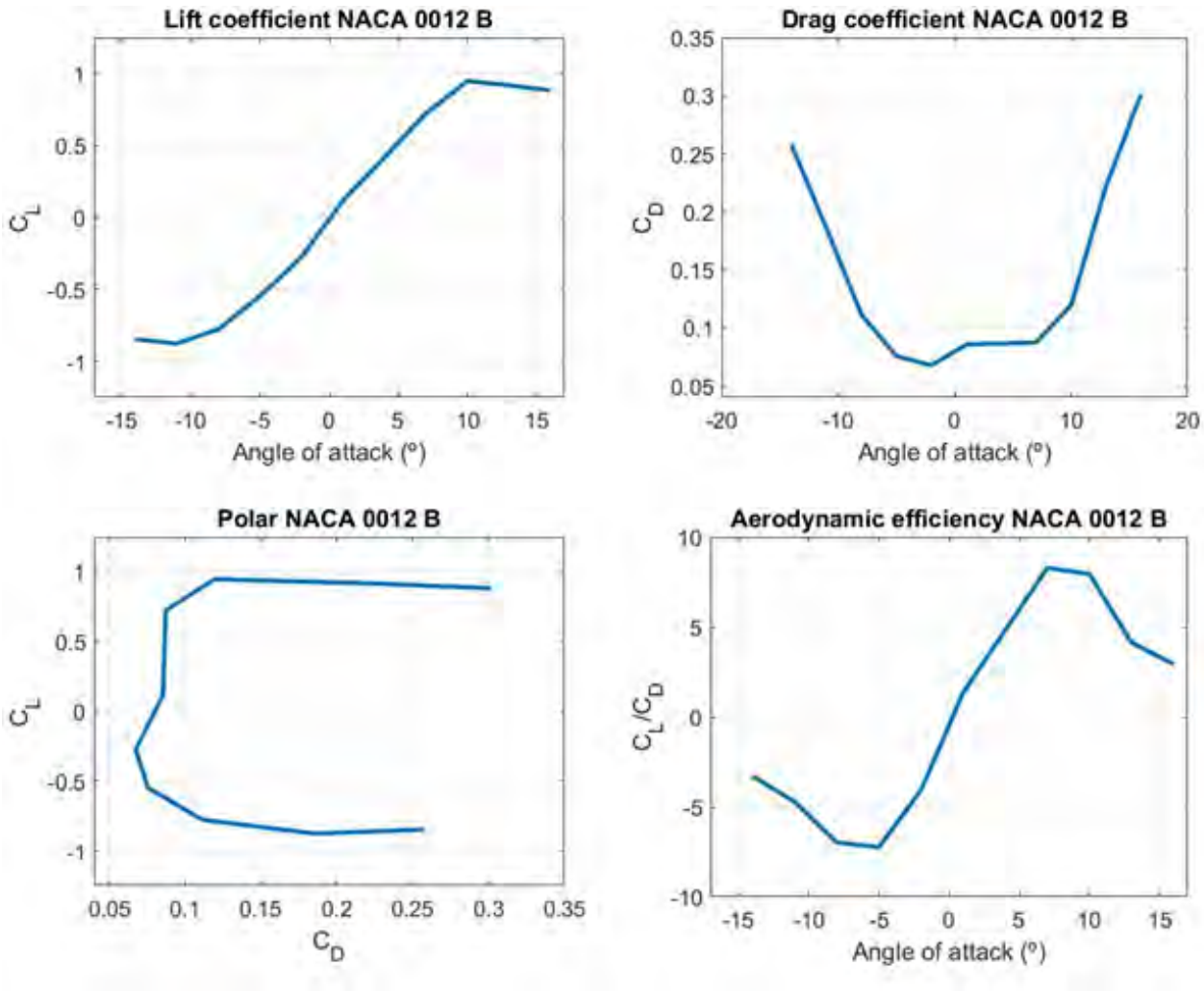

Figure 37: Results NACA 0012_B

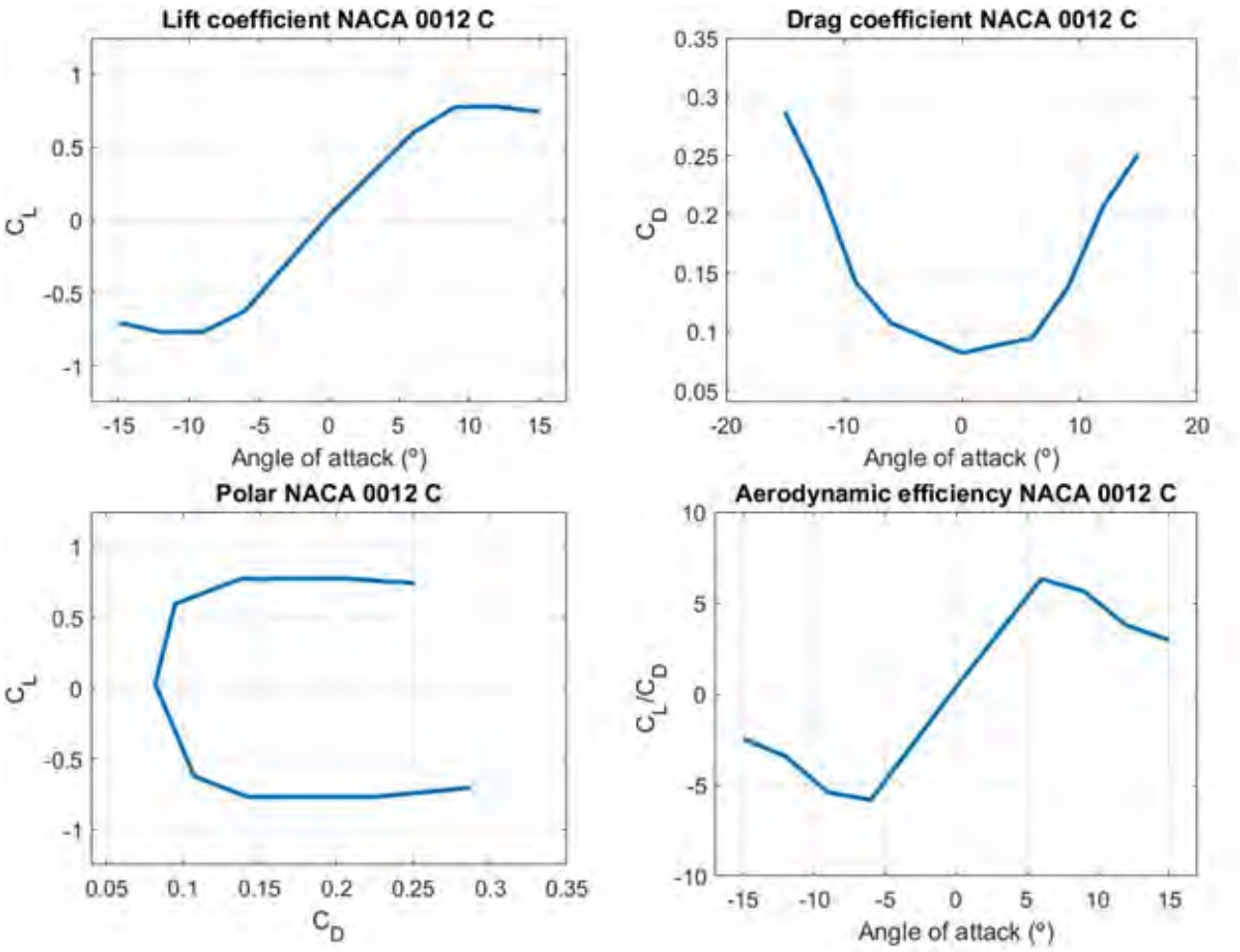

Figure 38: Results NACA 0012_C

Main and most important characteristic that can be observed in Figures 35 36 37 and 38 is the almost symmetric shape of the graphs. This is expected because a symmetric profile is being used, however is impossible to obtain perfect symmetric lines due to the great sources of errors from the measurement instruments and errors in the precision of the printers because is not possible obtain a perfectly symmetric airfoil. However the values obtained in all measurements have a great degree of agreement with the expected.

In all graphs where lift coefficient is represented, at 0°angle of attack near 0 lift is obtained, this was also anticipated.

About Stall, it appears near 10 for the four previous figures where lift coefficient is represented. But in the modified wings, the slope of the curve after stall is less, to see this better, later a comparison graph will be shown. When stall occurs, the wing starts to vibrate, resulting in a loss of information.

NACA 0012_A (Figure 36) has the greatest wave length of the modified wings so is expected to

have a behavior similar to the unmodified wing because the tubercles produce small influence in the wing. This time the scale reads high values of drag than the desired for small negative angles of attack and that will ends up in a non symmetric shape. One can notice that the maximum aerodynamic efficiency is near 10, very similar to the value reached in the unmodified NACA. In terms of lift this problem of asymmetry does not appear. Can be seen how the maximum lift coefficient is near 1 both in positive and negative angle of attack.

Behavior of NACA 0012_C and NACA0012_B is very similar between them, obtaining a near symmetric shape.

Before comparing all the wings some comments are done:

The non-symmetric behavior that is seen in all wings configurations is reasonable because is impossible to obtain a perfectly symmetric behavior. The reason could be the high source of errors that can appear in an experimental project. The tunnel produces very high vibrations that produce erroneous information in the scale. Establishing the correct value of the angle of attack is difficult because the angular spacing is small. The airfoil is not perfectly symmetric.

Regarding modified wings can be seen that in some points there is no information, for example in NACA 0012_C the wing was placed in 0°angle of attack and the following point was placed at 6°. This is done taking advantage of the linear behavior in the lift coefficient before stall appears, resulting in less time of measurement process. This is necessary because the amount of data needed is so large and the time of access to the facility is reduced.

8.1 Comparison

This section is one of the most important parts because a comparison between all wings will be done in order to see if the performance is improved or not.

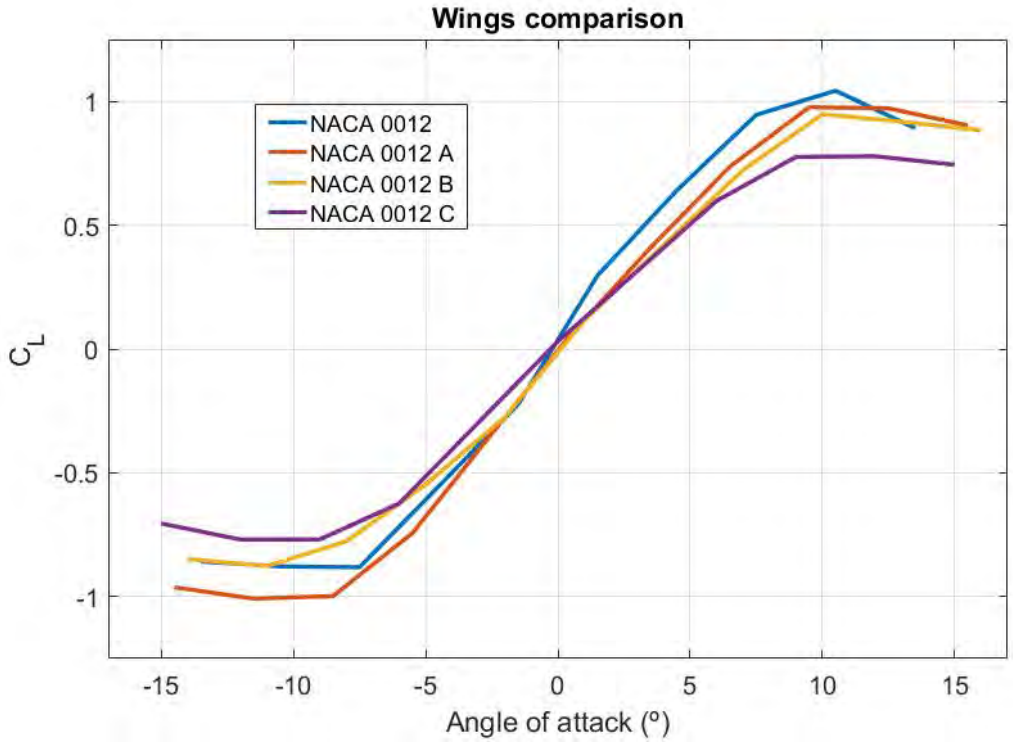

Figure 39: Comparison of lift coefficient between the four configurations

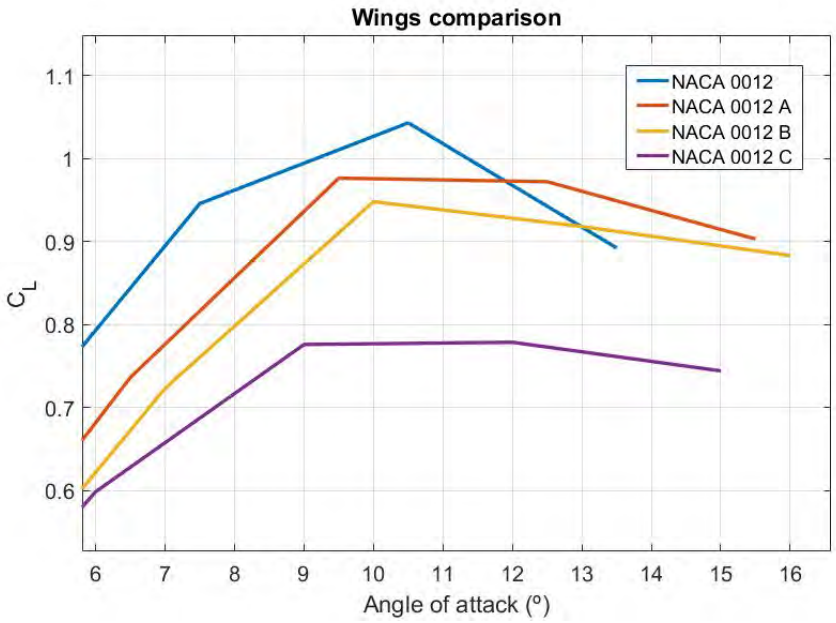

Figure 40: Lift coefficient comparison (detailed stall region)

Previous figures show the lift coefficient behavior versus angle of attack. The four wings crosses very near the 0 lift coefficient value at 0°angle of attack. The slope of pre-stall region in Figure 39 is near linear and very similar for all cases, because after stall is expected a behavior more or less similar, being a little bit worst for unmodified wings. However the main important part for this work is the stall region.

As stated in [42] and [5] the main contribution of tubercles leading edge is retard or soften the appearance of stall region of a wing. Taking a look in Figure 40 can be seen that unmodified NACA 0012 (blue line) is the wing that first suffers stall and have a more dramatic reduction in lift, because can be note that at 10°the lift coefficient of unmodified NACA decrease while in the modified wings still is maintained in its maximum value of lift coefficient. At this point is proved that stall is retarded and softened. Now a comparison between the modified profiles is developed in order to establish if there are a bound of tubercle configurations design.

To have a better and easier explanation of which configuration has a superior performance the amplitude-wavelength ratio presented in section 2.1 will help. From literature is established that as greater is the ratio, the maximum lift coefficient will be lower, but the stall region will be smoother, so the loss of lift is not dramatic.

Once stall appears, only data of next angles of attack to stall can be used. The reason has been explained before as a source of error, because when stall occurs, the wing starts to vibrate, these vibrations receive the name of stall buffeting [43], and end in wrong information recorded by the balance.

The conclusions adopted in [15] and [20] are corroborated with Figure 40, because comparing the yellow and purple line, which correspond to the middle and highest amplitude-wavelength

ratio respectively, with the red one, which correspond to the smallest amplitude-wavelength ratio, can be seen that the stall is more steeped when the ratio is smaller but the maximum lift coefficient is higher. It has sense because a smaller ratio means that the wing is nearer than the unmodified wing, because it has smaller amplitude or a high wavelength and the vortices generated in the tubercles are not important to produce the desired effect, however a higher ratio means tubercles which will generate stronger vortices. The difference between NACA 0012_B and NACA0012_C is not remarkable in terms on stall, it seems NACA0012_B to have a little worst performance when stall appears, but the maximum lift coefficient is much better for that wing.

[17] Said that the location of maximum thickness will affect the pre-stall region. If the maximum thickness appears at 50% of the chord, the tubercles has not influence in the lift in pre-stall region and post-tall is improve. However placing the maximum thickness at 30% of chord, as in this project, the lift in pre-stall region is penalized in expense to improve the post-stall regime.

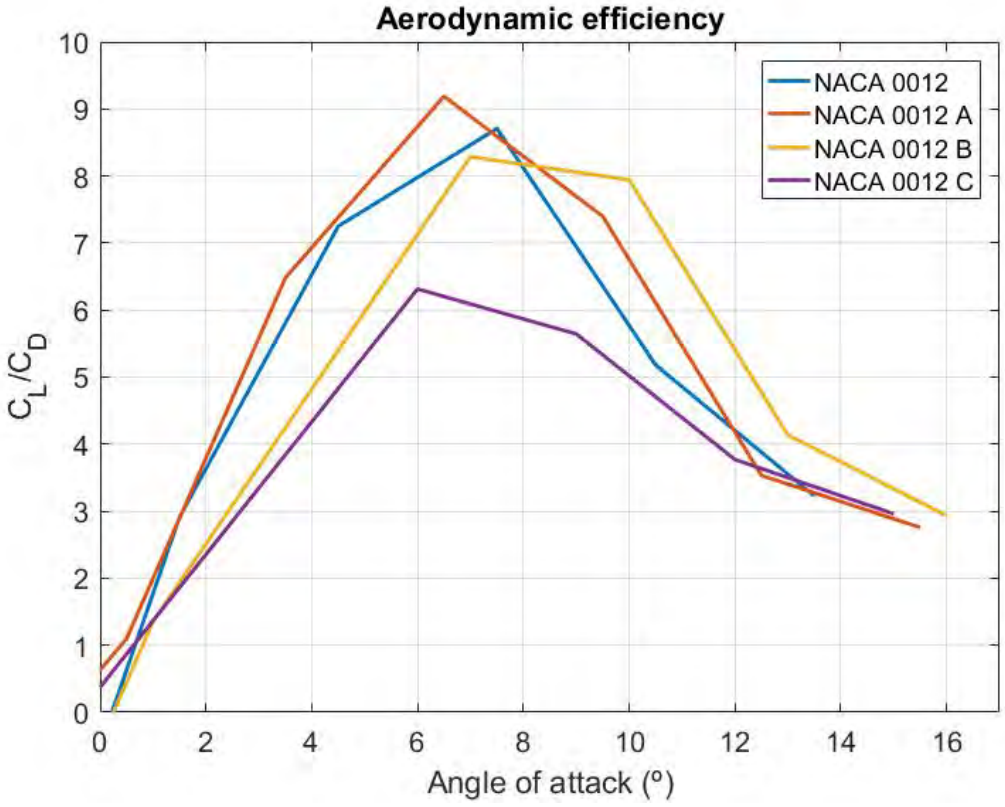

Figure 41: Aerodynamic efficiency comparison

The aerodynamic efficiency in NACA 0012_B and NACA 0012_C is usual that has a worse efficiency in the pre-tall region because as has been explained, the tubercles penalized the lift before stall appears. However once stall is passed, the performance of NACA 0012 worsen drastically. Efficiency of NACA 0012_A seems to be the best one. From literature NACA 0012

must has the best aerodynamic efficiency, however this change could be probably caused by the different material used. NACA 0012 was printed in ABS plastic and the modified wings with ceramic dust. Likely once the NACA 0012 was printed, starts to contract and suffering small deformations that cause a reduction in performance.

To conclude the results section is determine that the wings NACA 0012_C and NACA 0012_B have the best performance in the post-stall region as expected from the literature review.

9 Computational Fluid Dynamics (CFD)

From sections 2 to 8 all aspects related with experimental procedure such as experimental set up, corrections, fabrication of the model and results have been explained. At this point, to support the results, a study using computational fluid dynamics software is performed. For this project, open software is used, SimScale.

9.1 CFD introduction

The study of a fluid flow behavior is characterized mainly by its pressure and velocity field, which is composed by three components (u, v, w).

$$u(x, y, z, t) \qquad v(x, y, z, t) \qquad w(x, y, z, t) \qquad p(x, y, z, t)$$

To solve it, four equations are required. One equation is obtained from mass conservation and the three remaining from momentum conservation in each direction (x, y, z). These are the well know Navier-Stokes equations which can be solved for a small control volume (dx, dy, dz). There not exists an analytical solution for those equations, because are highly not linear coupled equations. In order to obtain a solution, a numerical method must be implemented, solving the equations for particular case at discrete points, this is known as Direct Numerical Solution (DNS) but the computational cost to solve it is huge so higher simplification is needed. For engineering purposes an average solution is enough, so a method called called Reynolds Average Navier Stokes (RANS) is applied. When solving this method a new term appears, the **Reynolds stress**. Reynolds stress should be solved through a series of equations provided by Reynolds, but those equations do not have analytical solution so different approximations are supply to find a good approximate results, the turbulence models. [44]

$$Reynolds\ \ stress \rightarrow \rho\overline{u_i' u_j'} \tag{25}$$

9.2 Turbulence model

There are several turbulence models. Depending on the complexity and specifications of the model one turbulence model or another is chosen. Also the computational cost must be considered when selecting the turbulence model, because there are models that need more powerful computers to solve the model. The most common are Spalart-Allmaras, K-epsilon, K-omega and Menter´s Shear stress Transport. Taking into account that in this project a very simple wing configuration is study, the K-omega turbulence model is selected, also because is one of the most commonly used. K-omega model is a two equation model which includes two extra transport equations to represent the turbulent properties of the flow. The name of the model came from the two variables needed to determine that turbulent properties: k and omega (ω)

- k→ turbulent kinetic energy, is the kinetic energy per unit of mass of the turbulent fluctuations in a turbulent flow:

$$k = \frac{1}{2}\left(\overline{u_x'^2} + \overline{u_y'^2} + \overline{u_z'^2}\right) = \frac{3}{2}\overline{u'^2} = \frac{3}{2}\left(U_\infty 0.16\, Re^{-1/8}\right)^2 = 0.58\, m^2/s^2 \tag{26}$$

- ω → is the rate at which turbulence kinetic energy is converted into thermal internal energy per unit volume and time.

$$\omega = \frac{\epsilon}{k\beta^*} = \frac{c_\mu^{3/4} k^{3/2} (0.7L)^{-1}}{k\beta^*} = 13.96 \tag{27}$$

Turbulence model information is obtained from [45] and [46].

9.3 Mesh

When solving the equations, a control volume is necessary, so two parts must be meshed, the body and the control volume.

SimScale software uses SnappyHexhMesh, which applies a particular method to generate the mesh. Once the geometry is imported and the control volume defined, both are divided in squares depending on the level of separation determined. If a square lies inside the body it is eliminated and if it lies in the control volume is maintained. So as the refinement level increases the squares lying in the bound between body and control volume fits better to the required shape.

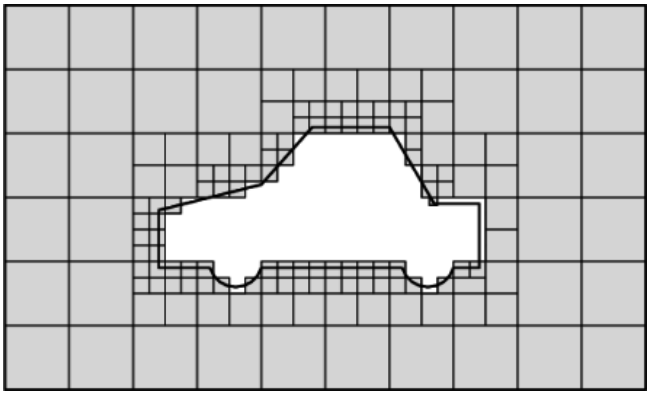

Figure 42: Example of mesh in SnappyHexMesh. Image taken from [47]

A refinement level determines who many times a square is divided following an exponential proportion. Two pictures are shown in order to have a better understanding of how the refinement levels works.

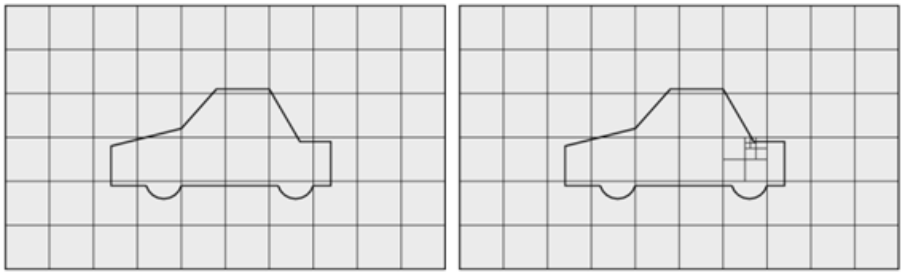

Figure 43: Refinement levels. Image taken from [47]

The left figure shows a base mesh with the entire elements with the smallest level of refinement. Looking at the right figure can be seen a square which is divided exponentially as the level of refinement is increased. A square is divided in 2^n squares, where n is the level of refinement.

The mesh is the key step in CFD because it will determine the computational cost, the validity of results and the accuracy. As finer is a mesh, better results will be obtained but a more powerful computer will be needed, however a less fine mesh will end in non reliable solutions but the time of computation will be less. So a trade-off must be done to find the optimal point of the mesh. To achieve it, a mesh convergence is done, which consist on compare the result of a characteristic value (for example C_L) for different meshes. Is expected that at some point of refinement, the value does not vary so much, assuming that the mesh is good enough to use it in the analysis.

Adding layers is necessary in the zone of fluid-solid interaction. It augments the original mesh to produce a smooth distribution along all walls. Wall Layers ensures adequate mesh across small gaps, which can be very difficult manually. Is known that at the walls, the velocity of the fluid is 0 and it grows through the boundary layer to reach the mean velocity of the free stream. The layers will represent the boundary layer, so the size of the boundary layer must be characterized. To build the layers correctly, the y+ value must be consider. y+ is a non- wall distance adimensionalized with the friction velocity, thickness of the first layer and kinematic viscosity. y+ vary depending on the turbulence model, for example the SST turbulence model has a y+ value smaller than one, that model will provide good results in terms on skin friction and roughness factor value. For the k-ω turbulence model, the one used in this work, the y+ value must be around 1, which is suitable for low Reynolds number analysis.

$$y^+ = \frac{\Delta y\, u_*}{\nu} = \frac{\Delta y}{\nu}\sqrt{\frac{\tau_w}{\rho}} \tag{28}$$

Is difficult to obtain the value of the first layer thickness, but on Internet there are y+ calculators [48] which given a desire y+ value, it calculates the value of the thickness for first layer. Once the first layer is known, is possible to construct the rest of the layers knowing an approximation size of the boundary layer thickness. When estimating boundary layer thickness, there is a good approximation called Blasius solution. The method is governed by an equation which assumes a linear growth of the layer with the position in the body. Is important to notice that

the theory is formulated to be applied over a flat plate, but it is also applicable over profiles [49]. Must be taken in consideration that this method is an approximation, and the curvature of the profile will differ from the result of a flat plate, but is assumed that this approach will give a good result for boundary layer thickness. For turbulent boundary layer the displacement thickness gets the form:

$$\delta(x) = 0.37 Re^{0.2} x \tag{29}$$

Introducing the reference length in x, is obtained:

$$\delta(c) = 0.37 \cdot 82000^{0.2} \cdot 0.08 = 0.003m \tag{30}$$

With this value and the thickness of the first layer obtained with [48] is possible to construct the boundary layer, introducing in SimScale the number of layers desired and the expansion ratio of the layers.

To study the mesh convergence, an angle of 4°is simulated. At the same time, the best mesh is going to be find and the value of the lift coefficient will be compare with the experimental results for the validation of the model. The way of simulating an angle of attack can be done by editing the geometry of the wing and placing it with the required angle of attack, but is easier changing the velocity components in SimScale with simpler trigonometric relations in order to emulate an angle of attack.

9.3.1 Mesh convergence

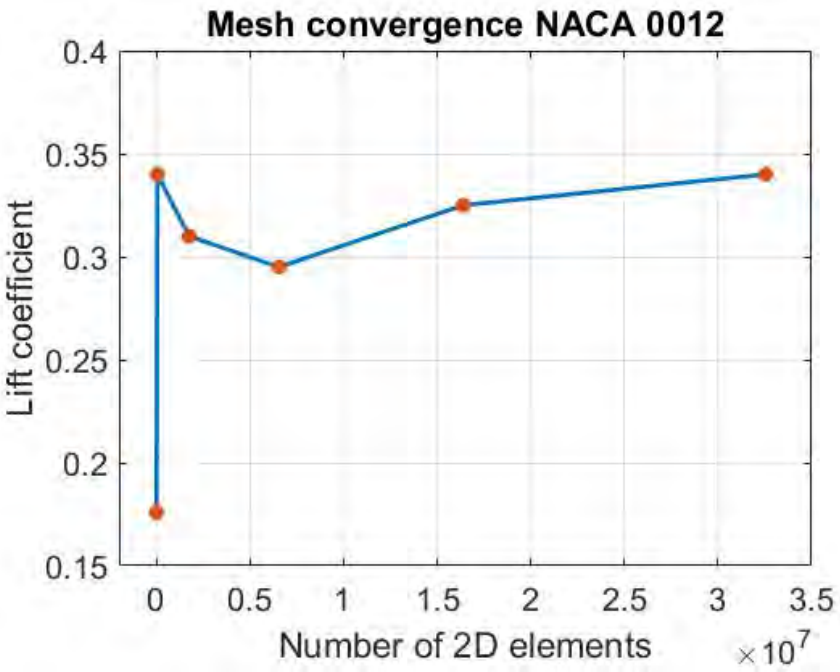

Figure 44: NACA 0012 Mesh convergence

Each red point in the graph equate to a mesh done in SimScale. The first mesh gives a very low value of Lift coefficient, but rapidly the values tend to converge to values between 0.3 and 0.35. The difference in elements between the last 2 points is more than 2 million of elements and the difference in lift is 0.015. This is a rise tendency that could end in more accurate values of lift coefficient, however increasing the number of elements end in an important increase of computational time. Is concluded that the mesh has reached a good level of convergence.

About the validation, experimental result of lift coefficient and the obtained in the software is displayed:

Database	SimScale	Deviation percentage
0.49	0.342	30%

Table 3: CFD model validation

There exist a difference of 30% between the database and the software output. This is an important variation between the CFD and experimental result. However the discrepancy can be accepted, because in the CFD analysis the wall is modeled completely attached to the wing tips, and in experiments splitter plats was used. So that difference is expected.

Also is important to consider that due to Reynolds number value, the study is framed in the transition regime, which could produce difficulties in the CFD analysis.

9.3.2 Mesh NACA 0012

Hereunder pictures of the mesh for the NACA 0012 will be shown.

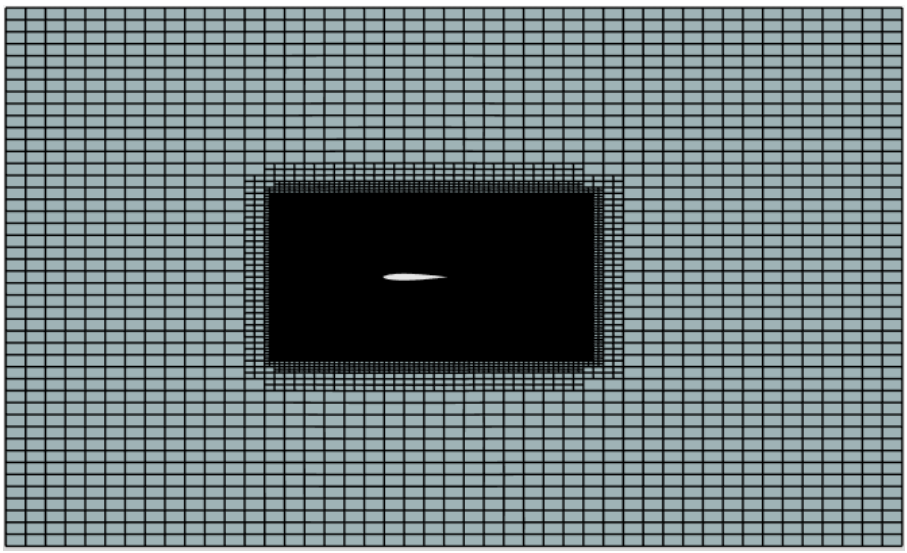

Figure 45: Mesh NACA 0012

Control volume is divided in 45 cells in horizontal direction and 45 in the vertical direction. Can be seen that the zone far away of the wing is not important because it does not provide relevant information so a less finer mesh can be done.

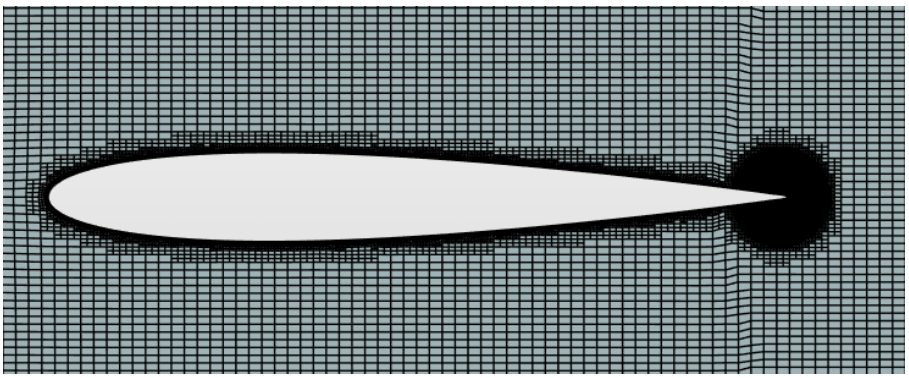

Figure 46: Detail of the NACA 0012 profile mesh

One can notice how as near the wing is, the mesh is more and more fine, because the information is more relevant.

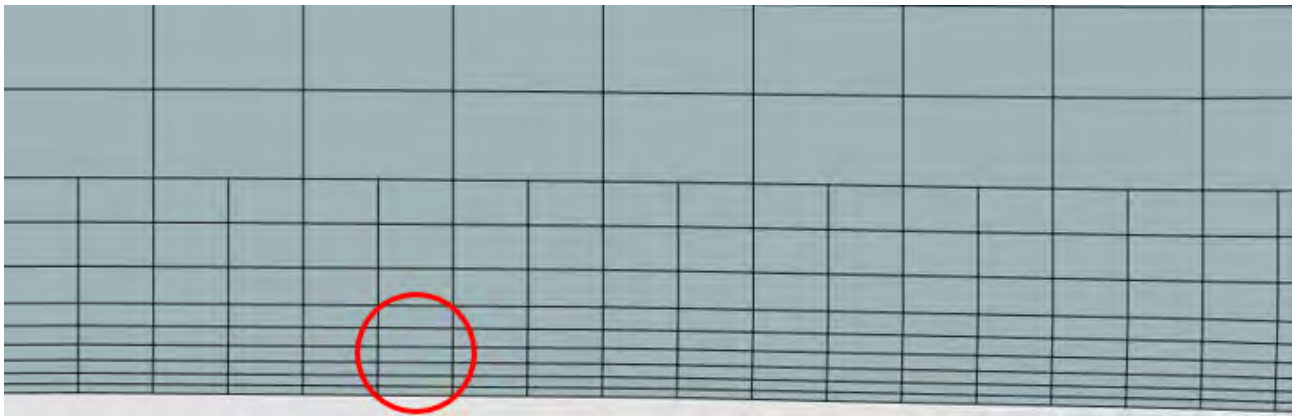

Figure 47: Layers details of NACA 0012

In previous figure there are 6 layers, forming the boundary layer. Inside the red circle, the 6 layers can be appreciated.

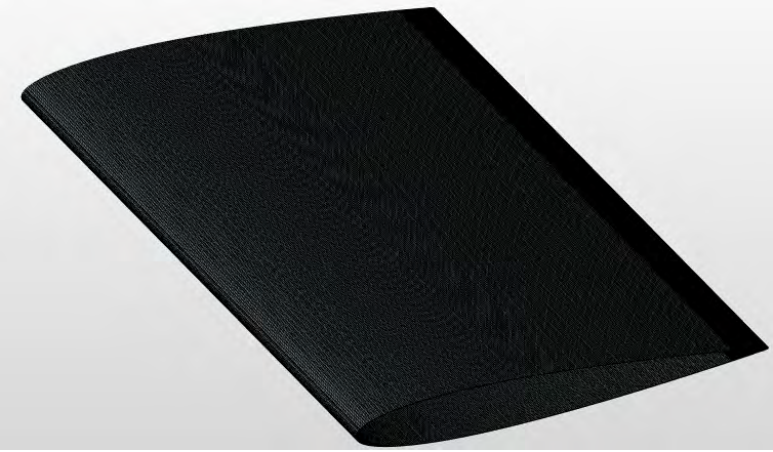

Figure 48: Wing mesh

9.3.3 Mesh NACA 0012_C

The mesh of tubercles wing is more difficult because the leading edge is no longer straight.

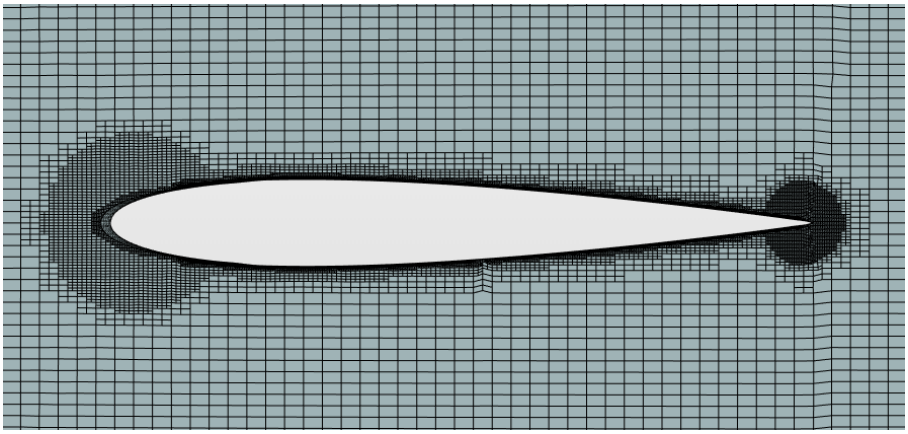

Figure 49: Profile Mesh of modified NACA

In Figure 49 appear two important zones which need a greater level of refinement, the tubercles and the trailing edge. The trailing edge needs a more accurate mesh because it ends in a cusp and it can produce problems to the mesh convergence. In the same way, leading edge tubercles need a greater refinement level due its complex shape.

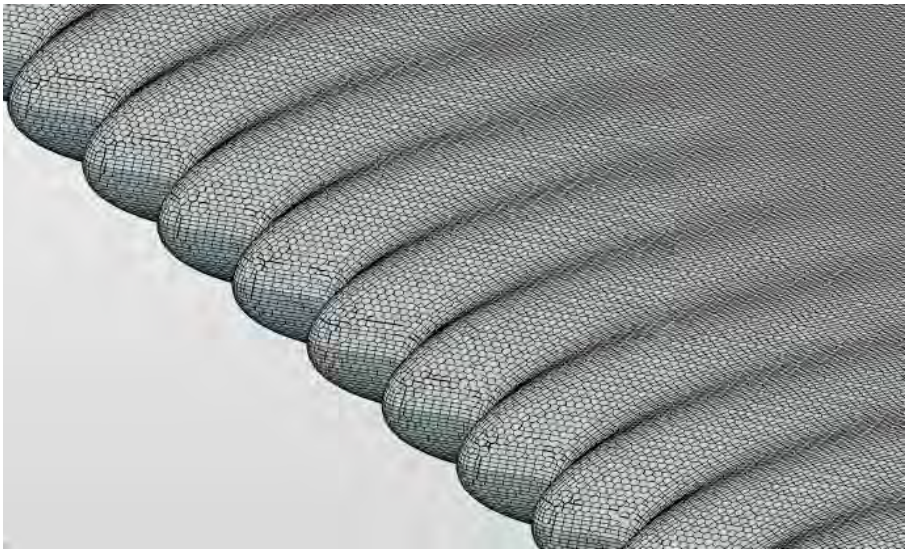

Figure 50: Tubercle Mesh

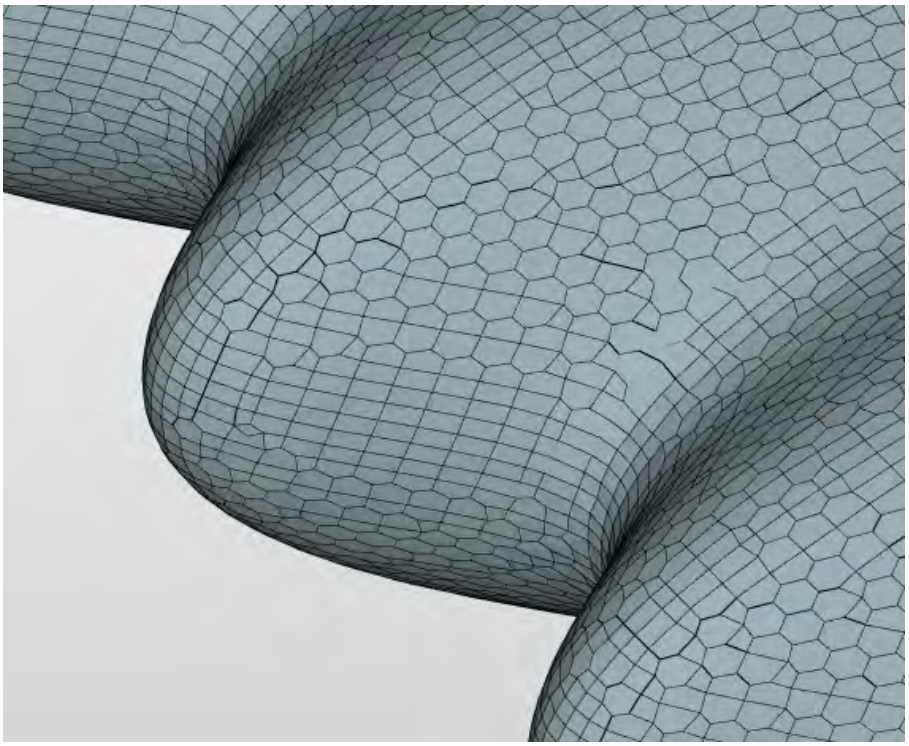

Figure 51: Tubercle mesh (detailed)

Surface refinement level of 7 is used in the wing surface. As can be seen it produces a very good result in terms of surface mesh because the shape of the tubercles is great reproduce.

9.4 Fluid properties

Inside the control volume air is introduced which the following properties:

Variable	Value
Density	$1.225 kg/m^3$
Viscosity model	Newtonian
Kinematic viscosity	$1.53\text{x}10^{-5} m^2/s$

Table 4: Fluid properties

9.5 Initial conditions

SimScale solves partial differential equations, so is necessary introduce initial conditions for the equations:

Initial condition	Value
Velocity	16 m/s
Pressure	101325 Pa
k	0.58 m^2/s^2
ω	13.96

Table 5: Initial conditions

9.6 Results

In this section the results are going to be displayed. Mainly the flow visualization will be shown, in order to support and complete the information obtained from the wind tunnel measurements. It is possible to made fluid visualization in the wind tunnel by means of smoke, particle seeding (PIV), Schlieren and tufts [50]. However flow visualization can be performed in CFD softwares, in this case SimScale which is an open software so the procedure will be cheaper than flow visualization in the tunnel and is not necessary access to the facility for more time than the used for the forces recording.

9.6.1 Pressure fields

SimScale´s post processor allows choosing different outputs. In this project is of interest know the pressure distribution, vorticity and wall shear stress to determine the separation.

9.6.1.1 NACA 0012 (profile) .

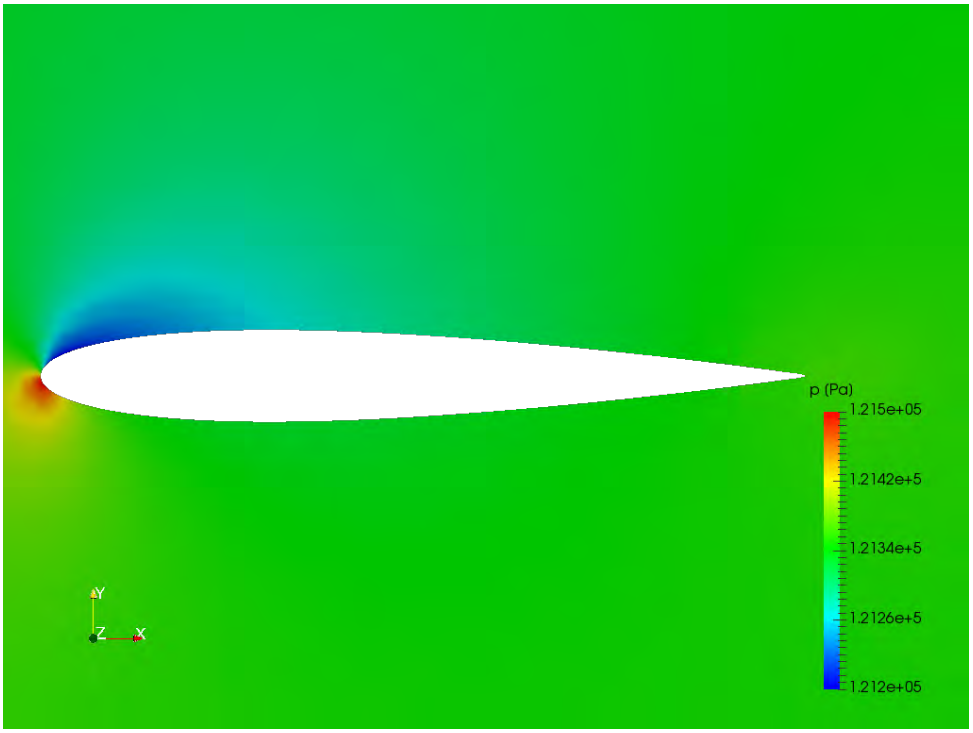

Figure 52: Pressure distribution over NACA 0012 Angle of attack 4°

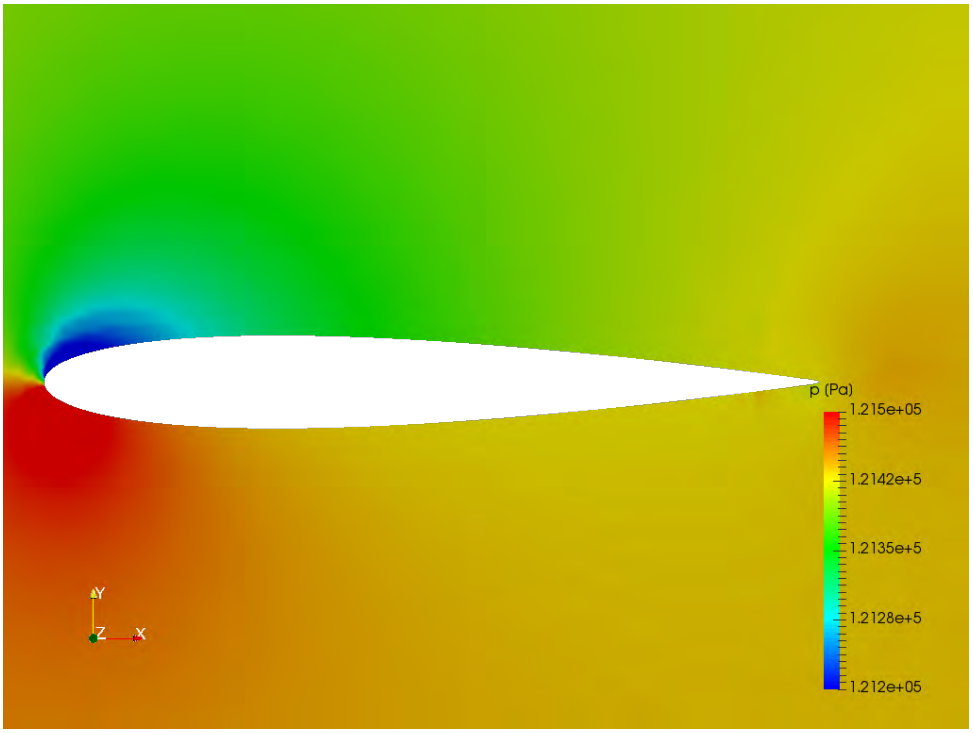

Figure 53: Pressure distribution over NACA 0012 Angle of attack 8°

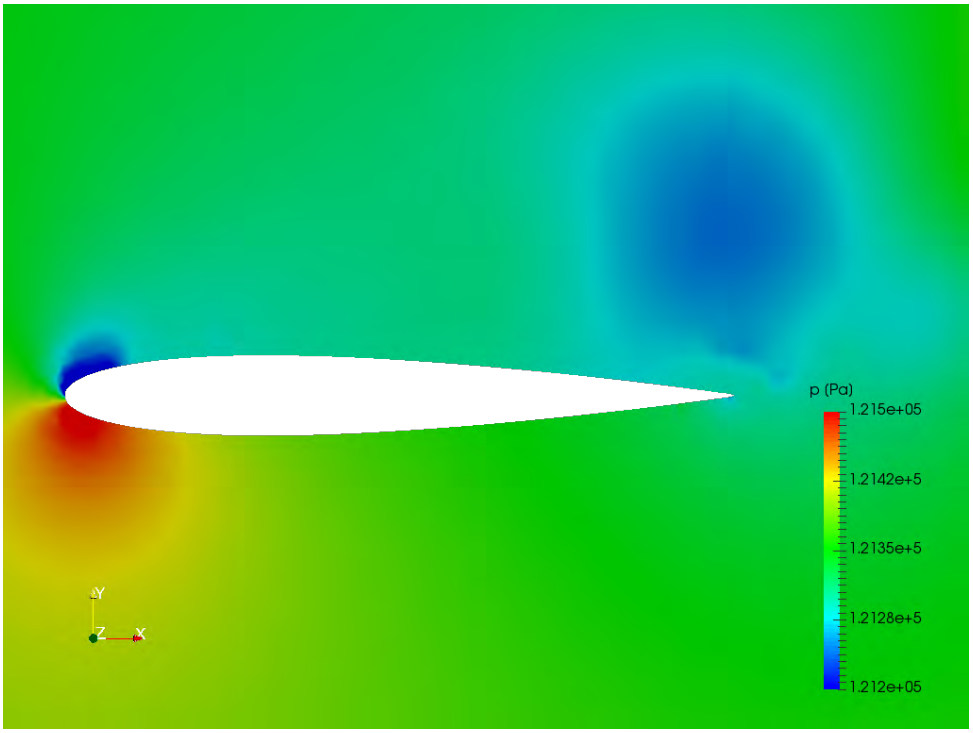

Figure 54: Pressure distribution over NACA 0012 Angle of attack 16°

Previous images show the evolution of pressure distribution as angle of attack increases. The figure corresponding to 4°presents a typical pressure distribution of NACA 0012 with a bubble of low pressure in the suction side of the leading edge and higher pressure in the pressure side. As stated in section 3 laminar separation bubble must appears, and comparing the images 53 and 54 it can be observed that for 8°the bubble is more concentrate in the leading edge, taking advantage that the point of separation can be known from [51] (≈8°) the bubble is near to explode and produce stall of the profile. However in the case of 16°, separation has been occurred which means that the bubble has been broken. Once separation occurs a characteristic pattern of eddies can be notice behind the bubble [33] that can be see in the big blue bubble which appears in the Figure 54. Also stall can be notice by the difference of pressure. In the case of 8°is greater than in 16°, as expected.

9.6.1.2 NACA 0012_C (profile) .

For the unmodified NACA is interested to see the pressure distribution in peaks and troughs:

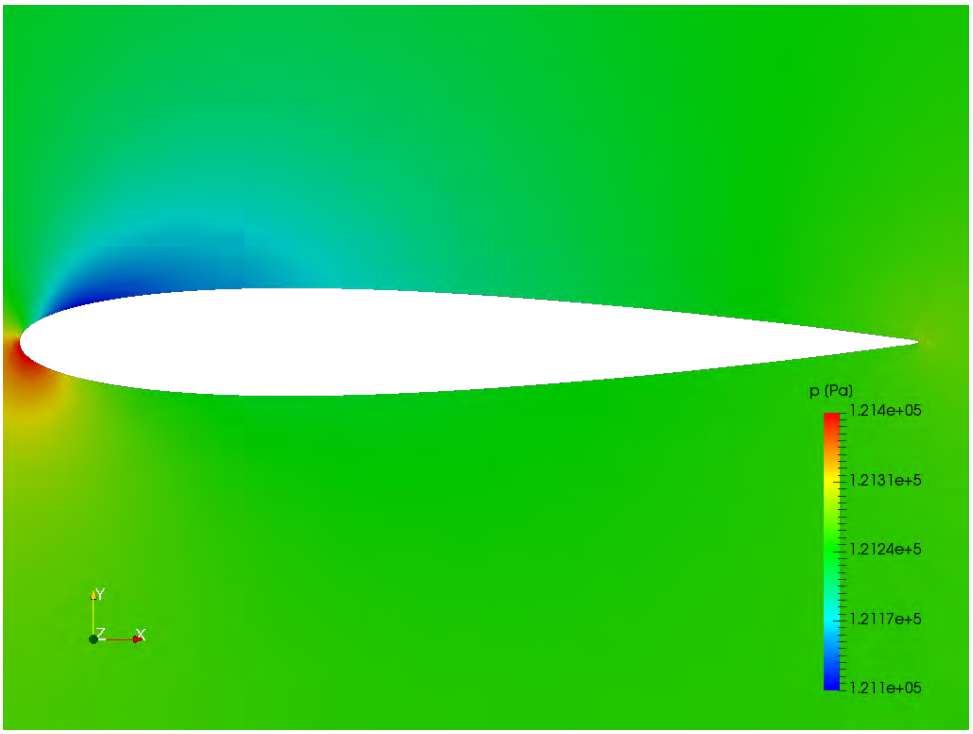

Figure 55: Pressure distribution at 4°angle of attack on peak

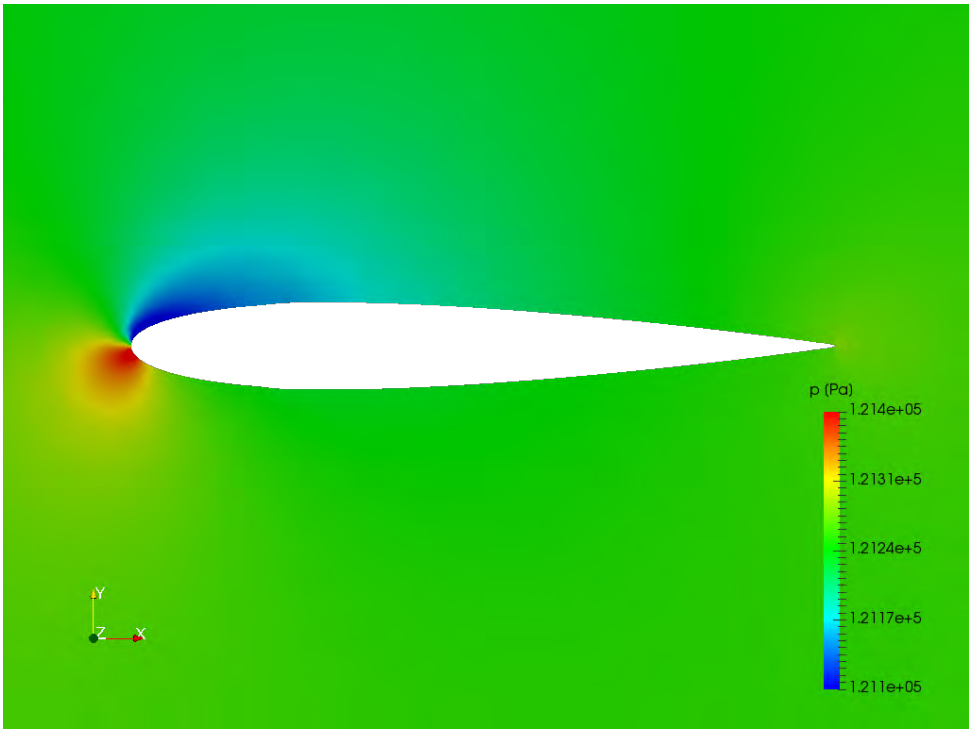

Figure 56: Pressure distribution at 4°angle of attack on trough

The pressure distribution in the peak is very similar to the one seen in the unmodified wing, with the leading edge bubble distributed approximately from 5% to 30% of the chord. Looking at the trough pressure distribution can be appreciated that the stagnation point is located at a different position than the peak profile as explained in [52]. In an unmodified wing, the stagnation line lies in the same point of the chord for the entire span, but the tubercles create a spanwise pressure distribution so it will change the chord position of the stagnation point.

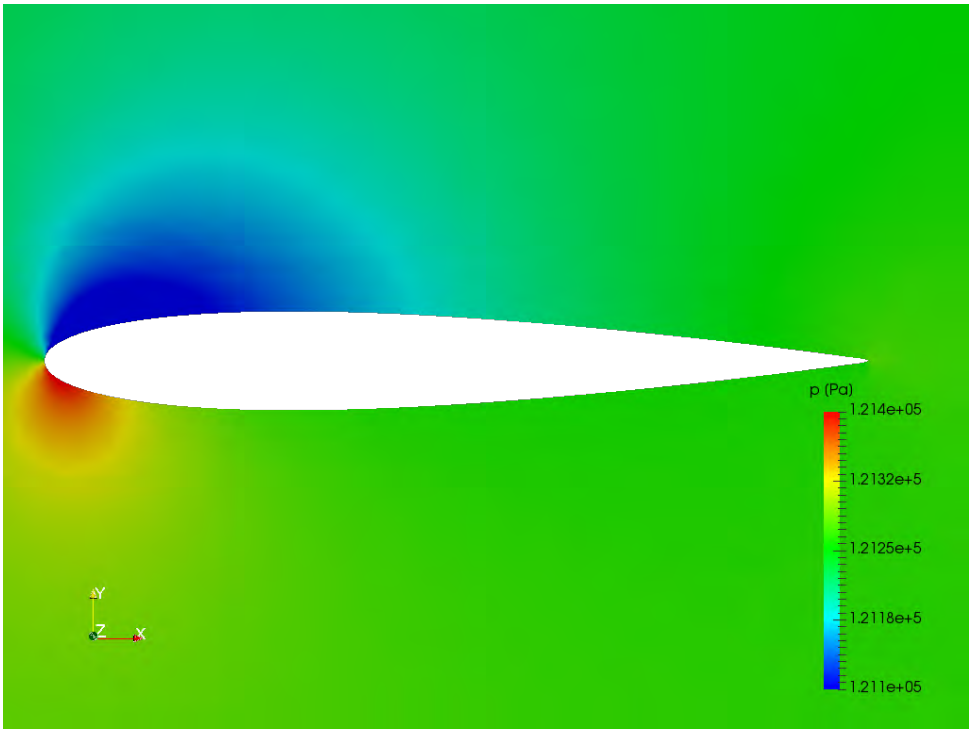

Figure 57: Pressure distribution at 8°angle of attack on peak

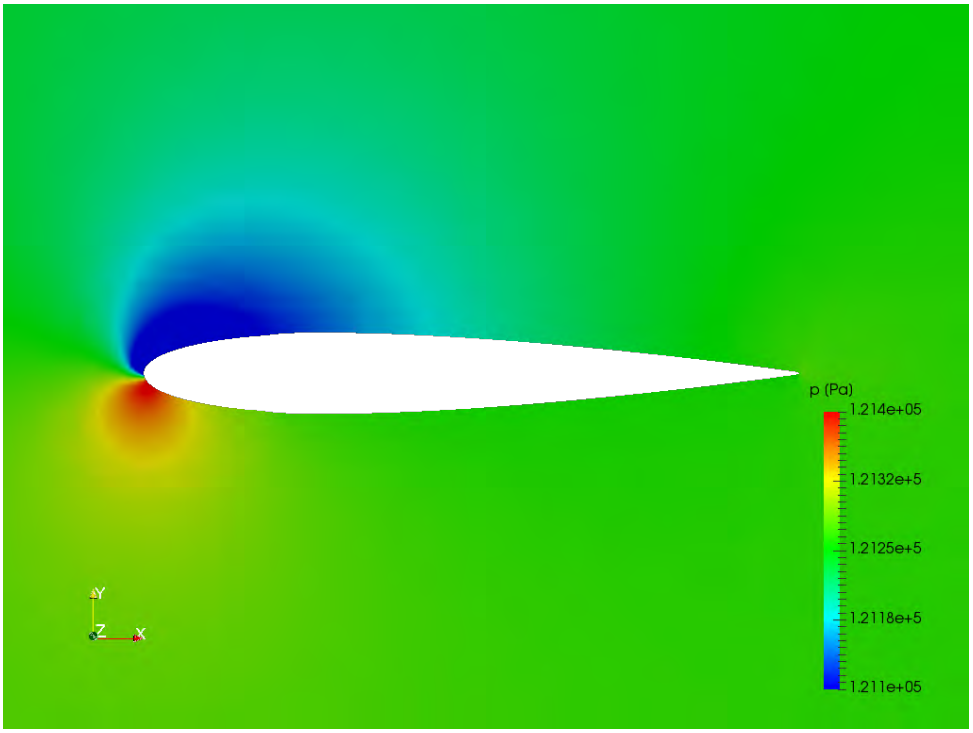

Figure 58: Pressure distribution at 8°angle of attack on trough

The more remarkable aspect for NACA 0012_C at 8°is the behavior of the bubble. In the unmodified case, the bubble has a smaller size and was practically blown out, but here is not appreciated a situation like that, and it has sense because in the peak no separation is seen. In the trough, the bubble affects a great part of the leading edge tip, and this allows to see very clear the position of the stagnation point in the trough.

9.6.1.3 NACA 0012_C (wing) .

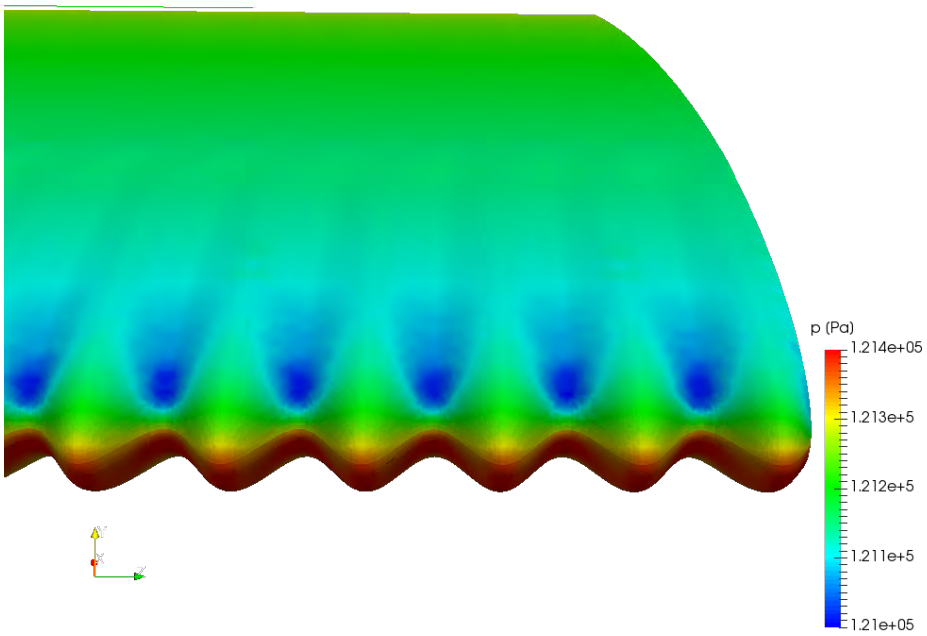

Figure 59: Pressure distribution over modified wing 4°Angle of attack

This picture allows to see more clearly the formation of vortices, because the low pressure zone in the troughs will produce it. The air passing across the peaks, will roll up because it goes from the zone of high pressure to low pressure.

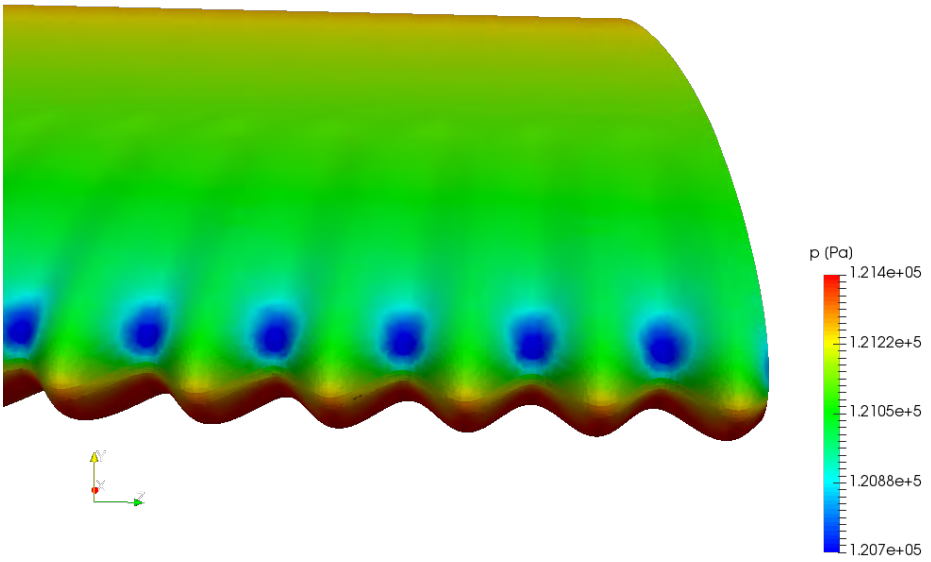

Figure 60: Pressure distribution over modified wing 8°Angle of attack

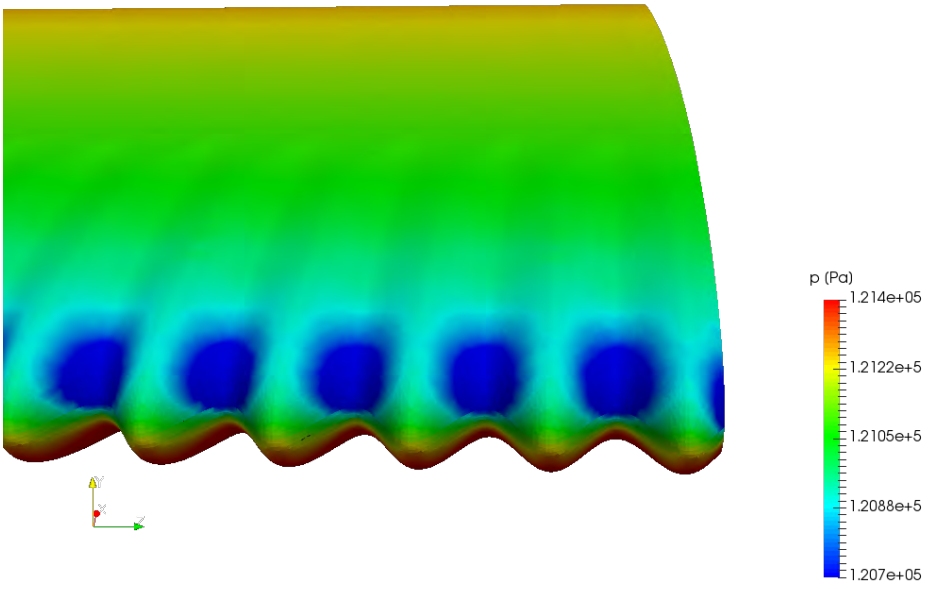

Figure 61: Pressure distribution over modified wing 11°Angle of attack

As angle of attack increases is possible to see that the pressure in the troughs is lower, so the flow will roll up with more intensity, increasing the circulation of the vortices.

9.6.2 Wall shear stress

Separation takes place when pressure gradient changes from favorable to adverse. At this inflexion point, the separation point can be found. Is possible locate it by looking at the wall shear stress:

$$\tau_w = \mu \left. \frac{\partial u}{\partial y} \right|_{y=0} \tag{31}$$

Taking into account the fact that separation point appears when $(\partial u/\partial y)_{y=0} = 0$, can be conclude that separation occurs when wall shear stress equals zero ($\tau_w = 0$) [53]. For the results of wall shear stress both wings will be displayed together for the same angle of attack in order to make easier the comparison of separation point.

Vorticity has also been analyzed.Is obtained a distribution of vorticity over the wing very similar to the wall shear distribution.

9.6.2.1 Angle of attack 4° .

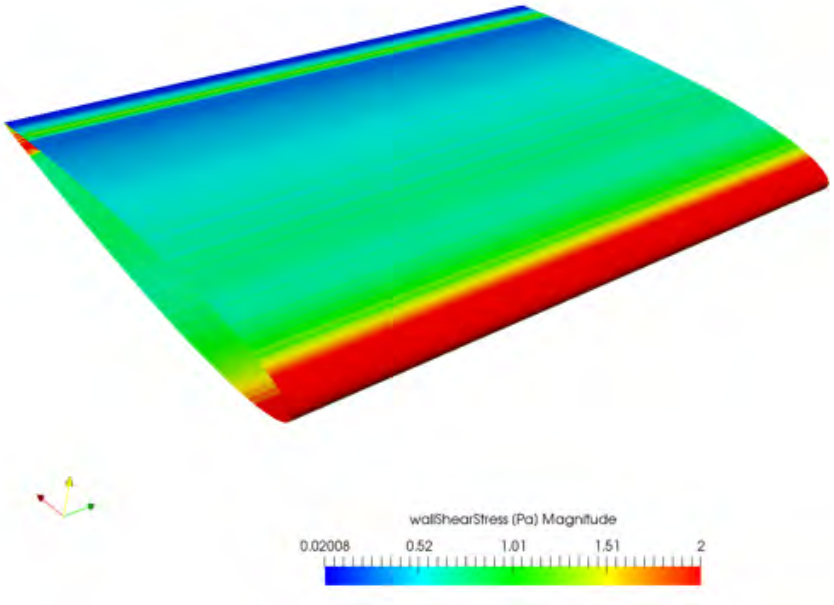

Figure 62: Wall shear stress NACA 0012 angle of attack 4°

Regarding previous figure can be seen that the flow is attached to the whole wing surface except near the trailing edge where seems to be separation produced by the flow leaving the wing.

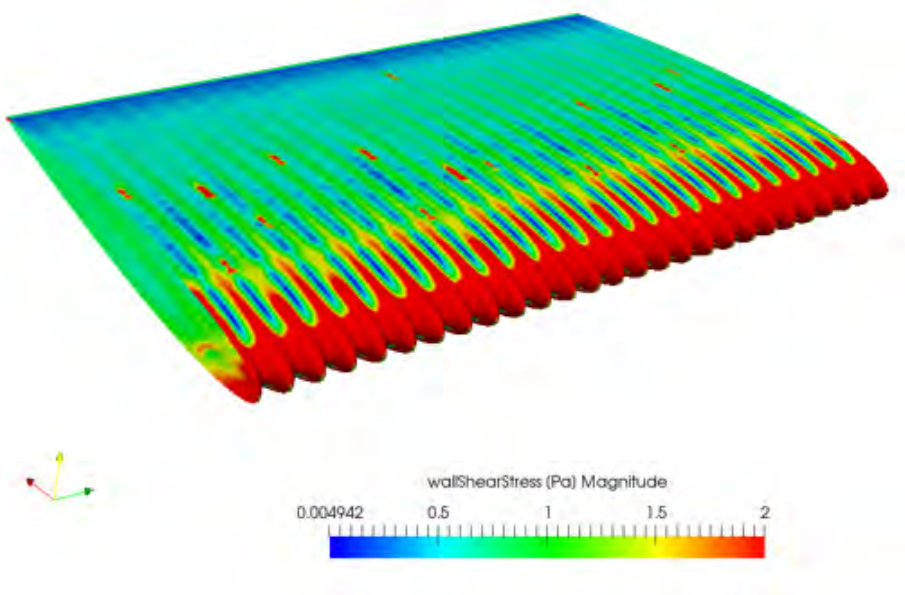

Figure 63: Wall shear stress NACA 0012_C angle of attack 4°

In respect of modified wing, is possible to see a characteristic pattern produce by the tubercles. In the tubercles, a small separation region can be notice, appearing after a reattachment in the back part of the suction side. There is not observed any separation point in the surface of the wing. Comparing the two figures the main difference is observed in the distribution of wall shear stress, but both wings are not stalled as expected. The behavior of the flow behind the trough is similar to the one described in [9]. With this angle of attack is not possible to see if the stall is delayed because both wings are not stalled, so is necessary make a study which NACA 0012 suffers stall and compare it with the modified wing.

9.6.2.2 Angle of attack 8° .

These results evaluations are very important in the project because is supposed that unmodified wing will stall near 8°so if the modified wing will not present stall a clear improvement could be attributed to the tubercles presence.

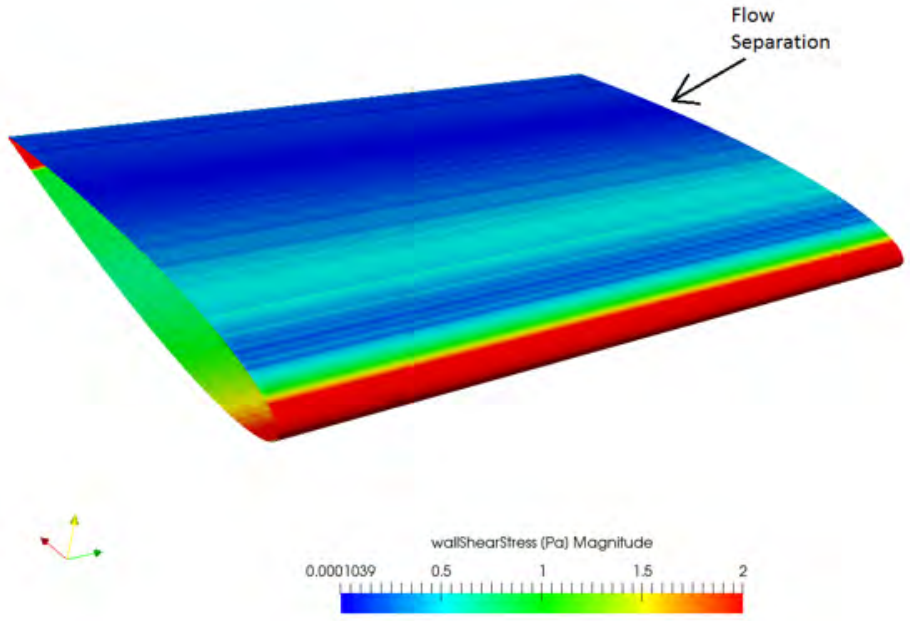

Figure 64: Wall shear stress NACA 0012 angle of attack 8°

In the previous figure is very clear that separation occurs at the wing surface, because in the highlighted zone, the value of wall shear stress is practically zero which corresponds to flow separation.

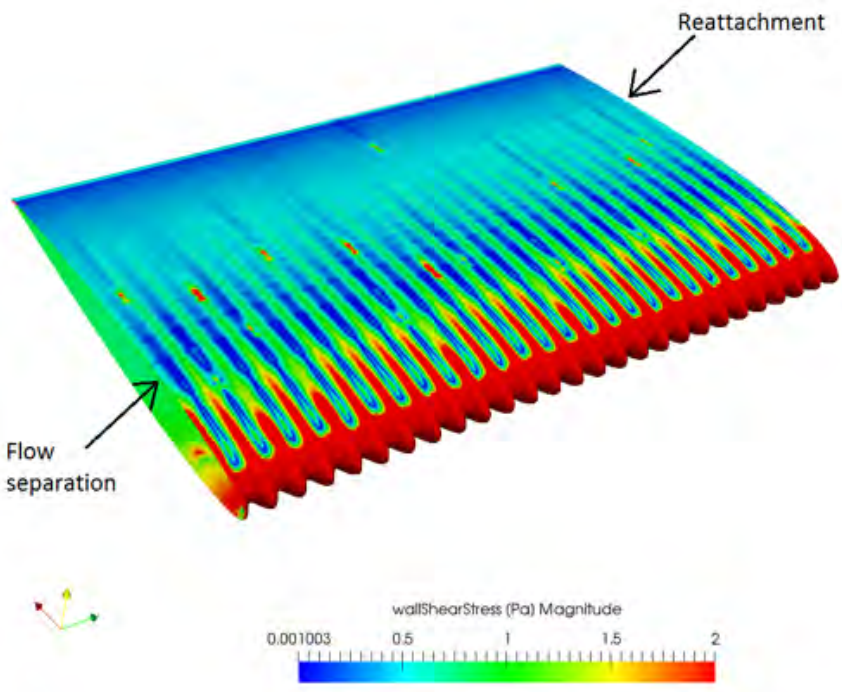

Figure 65: Wall shear stress NACA 0012_C angle of attack 8°

As the angle of attack increases the separation zone behind the tubercle´s trough is more evident, where the canopy should appears [9].Behind the peaks the flow is entirely attached over the entire wing surface. As expected once the flow reattaches, separation is not perceived on the wing, so is possible to establish that the wing of Figure 65 is not stalled. Remember that tubercles act as vortex generators, energizing the flow and retarding separation appearance.

This result is crucial for the investigation because can be proved that tubercles delays the angle of attack at which separation occurs as stated in [42] and [5]. Also CFD analysis has been provided a very good support to the results obtained in the wind tunnel.

10 Regulatory framework and socio-economic environment

During the data acquisition all the rules established in the law 31/1995, 8^{th} of November, prevention of working risks, have been followed. Technically this law is not applicable for the case of a student taking measurements in a laboratory, but exists an agreement to promote a Royal Ordinance which adapts the prevention of working risks law to those cases. Also the code of best practice guide approved by the governing board of the university has been followed.

Looking for applications, have been found a patented turbine and compressor using tubercles leading edge in the blades (Patent US20090074578).

Two of the software used (XFLR5 and SimScale) are Open source that means no costs. In addition is possible the access to public projects. This software present a great advantage for students because it reports good results and it has no costs for the user, and the huge amount of projects still are good for solving doubts and problems.

10.1 Costs

This table presents the breakdown of the cost associated to the project:

COSTS			
Resources	**€**	**Hours**	**Depreziation/Total€**
Wind tunnel	250000	35	7142,85
Ultimaker2+ extended	3000	20	150
Dust printer	100000	30	3333,33
ABS plastic	40	-	40
Scale	40000	35	1142,85
Amplifier	10000	35	285,71
DAS	2000	35	57,14
Computer	600	-	600
XFLR5	0	-	0
SimScale	0	-	0
Matlab (Student license)	50	-	50
CATIA (Student license)	82	-	82
Overleaf	0	-	0
Technician	15/hour	50	750
Engineer	15/hour	400	6000

Table 6: Cost breakdown

The total cost of the project is **19633.88€**

11 Conclusion and future works

To close the project, main conclusions and future works are presented.

After a literature review, three configurations of modified wings were chosen to study its difference from an unmodified NACA 0012. Creating an specific installation to measure forces in a wind tunnel. The main purpose of studying tubercle leading edge was demonstrate that it delays stall appearance.

Data collected in the experiments, allows to obtain some conclusions.

- Is demonstrated that tubercles can retard the appearance of stall as stated in [42] [5] [20] and [17]
- Inside of modified wing collection, was proved that as smaller the amplitude-wavelength ratio, softer the stall region is, it means a smoother loss of lift. This behavior is corroborated in [15] and [20]. Between NACA 0012_B and NACA 0012_C this difference is difficult to be seen, because the uncertainties and errors, together with the small variation in forces, complicates the comparison between both wings. However seems that NACA 0012_C has a better stall performance, but the aerodynamic efficiency is penalized so much, so for this experiment NACA 0012_B can be selected as the best one.

As can be seen, results have a significant level of agreement with previous validated experiments. Taking this into account, is possible to affirm that the installation provides correct data in experimental analysis. Usually buy an specific measurement instrument is something very expensive, but for this case, has been possible to create one with a 3D printer reducing considerable the cost. Of course that the precision of the printed one is much smaller than the others, but is possible to make a trade off between price and precision to get the optimal one. About wings, similar conclusion can be obtained, using the 3D printers has been possible to create a model to be tested.

Another important aspect obtained from this work is the importance of supporting and improving results with a simulated one, in this case using CFD analysis. With SimScale has been possible to see at what angle of attack separation occurs.

The validation of the installation leaves open the option of measure new configurations of wings or even a different project that involves measurement of forces.

Must be taken into consideration two main aspect of the experimental procedure: The geometry of the wing will produce small forces that are difficult to be measure because the variation is small. Maybe at some points the noise and the forces could be difficult to be differentiate. This, added to the common errors of an experimental analysis will lead to some discrepancies of the results, however the data obtained in the project have been seen to be accurate enough. One possibility proposed to avoid this problem of small forces, is repeat the measurements in a water tunnel, where due to higher density of water, will increase forces by a factor 10.

Another work propose, consist on repeat the experiments at different Reynolds number values,

with the same configurations and see if the discrepancies are consistent.

With respect to the behavior of the tubercle leading edge wing, have been clearly seen that an improvement in the aerodynamic performance (in terms of stall) can be attributed to the tubercles which act as vortex generators.

References

[1] "European Commission" 6 February 2018,[Online].Available: https://ec.europa.eu/clima/policies/transport/aviation. [Accessed March 2017].

[2] "Clean Sky" [Online]. Available: http://www.cleansky.eu/benefits. [Accessed March 2017].

[3] S. Hecht and J. M. Fréchet, (2001), "Dendritic Encapsulation of Function: Applying Nature's Site Isolation Principle from Biomimetics to Materials Science". *Anegewandte Chemie International Edition*, Ed. 40, pp. 74–91

[4] "Velcro" [Online]. Available: https://www.velcro.es/about-us/history/. [Accessed March 2017].

[5] F. E. Fish, P. W. Weber, M. M. Murray and L. E. Howle, "The Tubercles on Humpback Whales' Flippers: Application of Bio-Inspired Technology". *Integrative and Comparative Biology*, vol.51, no.1,pp. 203-213, 2011.

[6] F. E. Fish and G. V. Lauder, "Passive and Active Flow Control by Swimming Fishes and Mammals" *Annual Reviews*, vol.38, pp. 193-224 2006.

[7] "National Geographic" https://www.nationalgeographic.com/animals/mammals/h/humpback-whale/. [Accessed March 2017].

[8] E. Livya, G. Anitha, P.Valli "Aerodynamic Analysis of Dimple Effect on Aircraft Wing". *World Academy of Science, Engineering and Technology International Journal of Aerospace and Mechanical Engineering*. vol.9, No.2, pp. 350-353.

[9] P. W. Weber, L. E. Howle, M. M. Murray and D. S. Miklosovic, "Computational Evaluation of the Performance of Lifting Surfaces With Leading-Edge Protuberances" *Journal of aircraft*. vol.48, no.2, 2011.

[10] J. Favier, A. Pinelli and U. Piomelli, "Control of the Separated Flow Around an Airfoil Using a Wavy Leading Edge Inspired by Humpback Whale Flippers" *Comptes Rendus Mécanique*. vol.340, pp. 107-114, 2012.

[11] Z. Wei, T. H. New and Y. D. Cui, "An Experimental Study on Flow Separation Control of Hydrofoils with Leading-Edge Tubercles at Low Reynolds Number". *Ocean Engineering*. vol.108, pp. 336-349, 2015.

[12] K. L. Hansen, N. Rostamzadeh, R. M. Kelso and B. B. Dally, "Evolution of the Streamwise Vortices Generated Between Leading Edge Tubercles". *Journal of Fluid Mechanics*. vol.788, pp. 730-766, 2015.

[13] K. D. Visser and R. C. Nelson, "Measurements of Circulation and Vorticity in the Leading-Edge Vortex of a Delta Wing" *AIAA Journal*. vol.31, no.1, 1993.

[14] E. A. van Nierop, S. Alben and M. P. Brenner, "How Bumps on Whale Flippers Delay Stall: An Aerodynamics Model". *Physical Review Letters*. vol.100, 2008.

[15] D. Custodio, C. W. Henoch and H. Johari, "Aerodynamic Characteristics of Finite Span Wings with Leading-Edge Protuberances". *AIAA Journal*. vol.53, no.7, pp. 1878-1893, 2015.

[16] Z. Wei, B. Zang, T. H. New and Y. D. Cui, "A Proper Orthogonal Decomposition Study on the Unsteady Flow Behavior of a Hydrofoil with Leading-Edge Tubercles". *Ocean Engineering*. vol.121, pp. 256-368, 2016.

[17] K. L. Hansen, R. M. Kelso and B. B. Dally, "Performance Variations of Leading-Edge Tubercles for Distinct Airfoil Profiles". *AIAA Journal*. vol.49, no.1, pp. 185-194, 2011.

[18] A. A. Gawad, "Utilization of Whale-Inspired Tubercles as a Control Technique to Improve Airfoil Performance". *Transition on Control and Mechanical System*. vol.2, no.5, pp. 212-218, 2013.

[19] K. Hansen, R. Kelso and C. Doolan, "Reduction of Flow Induced Airfoil Tonal Noise Using Leading Edge Sinusoidal Modifications". *Acoustics Australia*. vol.40, no.3, pp. 172-177, 2012.

[20] S. M. Aftab, N. A. Razak, A. S. Mohd Rafie and K. A. Ahmad, "Mimicking the Humpback Whale: An Aerodynamic Perspective". *Progress in Aerospace Sciences.*, vol.84, pp. 48-69, 2016.

[21] C. L. Ladson, "Effects of Independent Variation of Mach and Reynolds Numbers on the Low-Speed Aerodynamic Characteristics of the NACA 0012 Airfoil Section". *NACA Technical Memorandum 4074*. 1988.

[22] E. V. Laitone, "Wind Tunnel Tests of Wings at Reynolds Numbers Below 70000". *Experiments in Fluids*. vol.23, pp. 405-409, 1997.

[23] R. E. Sheldahl and P. C. Klimas, "Aerodynamic Characteristics of Seven Symmetrical Airfoil Sections Through 180-Degree Angle of Attack for Use in Aerodynamic Analysis of Vertical Axis Wind Turbines". 1981.

[24] J. B. Barlow, W. H. Rae,Jr and A. Pope, "Low-Speed Wind Tunnel Testing" John Wiley & Sons, 1999.

[25] "UIUC Applied Data Site" [Online]. Available: http://mselig.ae.illinois.edu/ads/coord_database.html. [Accessed June 2017].

[26] "Hofstra group" [Online]. Available: https://www.hofstragroup.com/product/kistler-9257b-triaxial-force-sensor-load-cell/. [Accessed January 2018]

[27] C. "Wind Turbine Project Lift, Drag, Blade Aerodynamics & Power". 2014.

[28] J. Katz, Low Speed Aerodynamics, Cambridge University press, 2001.

[29] A. Barrero , J. Meseguer and A. Sanz, Aerodinámica de altas velocidades, Madrid: Garceta, 2011.

[30] "Smart Blade," [Online]. Available: http://smart-blade.com/research-activity/wind-tunnel-measurements.html. [Accessed December 2017].

[31] "National Aeronautics and Space Administration"[Online]. Available: https://www.grc.nasa.gov/www/BGH/reynolds.html. [Accessed December 2017].

[32] R. M. King, "Study of an Adaptive Mechanical Turbulator for Control of Laminar Separation Bubbles" 2001.

[33] M. Jahanmiri, "Laminar Separation Bubble: Its Structure, Dynamics and Control". Department of Applied Mechanics, Chalmers University of Technology, Göteborg, 2011.

[34] "Imprimalia 3D" [Online]. Available: http://imprimalia3d.com/impresoras3d/zprinter-450. [Accessed February 2018].

[35] "XFLR5," [Online]. Available: http://www.xflr5.com/docs/Acerca%20de%20XFLR5%20%20V6.03.pdf. [Accessed December 2017].

[36] "Wiremeshes" [Online]. Available: http://www.wiremeshes.eu/. [Accessed December 2017].

[37] NASA, "Low Reynolds Number Airfoil Survey (Volumen I)" Virginia, 1982.

[38] J. G. Herriot, "Blockage Corrections for Three Dimensional-Flow Closed-Throat Wind Tunnels with Consideration of the Effect of Compressibility" *NASA*. 1950.

[39] E. C. Maskell, "A Theory of the Blockage Effects on Bluff Bodies and Stall Wings in a Closed Wind Tunnel". *Reports and Memorandum* no.3400, 1963.

[40] R. J. Moffat, "Describing the Uncertainties in Experimental Results" 1988.

[41] "Investopedia" [Online]. Available: https://www.investopedia.com/terms/s/standarddeviation.asp. [Accessed January 2018].

[42] D. S. Miklosovic, M. M. Murray, L. E. Howle and F. E. Fish, "Leading-Edge Tubercles Delay Stall on Humpback Whale (Megaptera Novaeangliae) Flippers". *Physics of Fluids*. vol.16, no.5, pp. 39-42, 2004.

[43] "Space Safety Magazing" [Online]. Available: http://www.spacesafetymagazine.com/aerospace-engineering/spacecraft-design/what-is-a-stall/. [Accessed January 2018].

[44] "Learnengineering" [Online]. Available: http://www.learnengineering.org. [Accessed January 2018].

[45] "CFD Online," [Online]. Available: https://www.cfd-online.com. [Accessed December 2017].

[46] "Afs," [Online]. Available: http://www.afs.enea.it. [Accessed December 2017].

[47] "Open Foam Guide User," [Online]. Available: https://www.openfoam.com/documentation/user-guide/. [Accessed January 2018].

[48] "Pointwise," [Online]. Available: http://www.pointwise.com/yplus/. [Accessed January 2018].

[49] "Viscous Flow Along a Wall," Standford University Department of Aeronautics and Astronautics.

[50] "National Aeronautics ans Space Department," [Online]. Available: [https://www.grc.nasa.gov/www/k-12/airplane/tunvis.html. [Accessed January 2018].

[51] "Airfoil Tools," [Online]. Available: http://airfoiltools.com/. [Accessed January 2018].

[52] P. Watts and F. E. Fish, "The Influence of Passive, Leading Edge Tubercles on Wing Performance".

[53] S. M. Fielding, "Laminar Boundary Layer Theory". Durham University, 2015.

Annexes

Annex A

Specifications

Printer and printing properties

Technology	Fused deposition modeling (FDM)
Print head	Single-extrusion print head with swappable nozzles
Build volume	223 x 223 x 305 mm
Filament diameter	2.85 mm
Layer resolution	0.25 mm nozzle: 150 to 60 micron 0.40 mm nozzle: 200 to 20 micron 0.60 mm nozzle: 400 to 20 micron 0.80 mm nozzle: 600 to 20 micron
XYZ accuracy	12.5, 12.5, 5 micron
Print head travel speed	30 to 300 mm/s
Build speed	0.25 mm nozzle: up to 8 mm^3/s 0.40 mm nozzle: up to 16 mm^3/s 0.60 mm nozzle: up to 23 mm^3/s 0.80 mm nozzle: up to 24 mm^3/s
Build plate	Heated glass build plate
Build plate temperature	50 - 100 °C
Build plate leveling	Assisted leveling process
Supported materials	PLA, ABS, CPE, CPE+, PC, Nylon, TPU 95A, and PP
Nozzle diameter	0.25, 0.40, 0.60, and 0.80 mm nozzles (included)
Nozzle temperature	180 - 260 °C
Nozzle heat up time	~ 1 minute
Build plate heat up time	< 4 minutes
Operating sound	50 dBA
Connectivity	Standalone 3D printing from SD card (included)

Physical dimensions

Dimensions	342 x 357 x 488 mm
Dimensions (with bowden tube and spool holder)	342 x 493 x 688 mm
Nett weight	12,3 kg
Shipping weight	19,5 kg
Shipping box dimensions	400 x 395 x 645 mm

Power requirements

Input	100 - 240 V 4 A, 50 - 60 Hz
Output	221 W max. 24 V DC, 9.2 A

Ambient conditions

Operating ambient temperature	15 - 32 °C See material specifications for optimal conditions
Non-operating temperature	0 - 32 °C

Software

Supplied software	Cura, our free print preparation software
Supported OS	MacOS, Windows, and Linux
File types	STL, OBJ, X3D, and 3MF G and GCODE BMP, GIF, JPG, and PNG

Annex B

Force

KISTLER
measure. analyze. innovate.

Multicomponent Dynamometer

Type 9257B

–5 ... 10 kN, Top Plate 100x170 mm

Quartz three-component dynamometer for measuring the three orthogonal components of a force. The dynamometer has a great rigidity and consequently a high natural frequency. Its high resolution enables the smallest dynamic changes in large forces to be measured.

- Universal applicable
- For cutting force measurements
- Stable and reliable

Description

The dynamometer consists of four three-component force sensors fitted under high preload between a baseplate and a top plate. Each sensor contains three pairs of quartz plates, one sensitive to pressure in the z direction and the other two responding to shear in the x and y directions respectively. The force components are measured practically without displacement.

The outputs of the four built-in force sensors are connected inside the dynamometer in a way to allow multicomponent measurements of forces and moments to be performed. The eight output signals are available at the 9-conductor flange socket.

The four sensors are mounted ground-insulated. Therefore ground loop problems are largely eliminated.

The dynamometer is rustproof and protected against penetration of splashwater and cooling agents. Together with the connecting cable Type 1687B5/1689B5 and Type 1677A5/1679A5 it corresponds to the protection class IP67.

A special thermal isolation coating is integrated in the top plate which renders the dynamometer largely insensitive to temperature influences.

Application Examples

- Dynamic and quasistatic measurement of the three orthogonal components of a force
- Measuring cutting force when turning, milling, grinding etc. In conjunction with the calibrated partial ranges the high sensitivity and low threshold allow exact measurements on small tools and when grinding.
- Measurements on scale models in wind channels

Technical Data

Range	F_x, F_y, F_z	kN	–5 ... 5 [1]
F_z for F_x and $F_y \leq 0{,}5\ F_z$	F_z	kN	–5 ... 10 [2]
Calibrated partial range 1	F_x, F_y	N	0 ... 500
	F_z	N	0 ... 1 000
Calibrated partial range 2	F_x, F_y	N	0 ... 50
	F_z	N	0 ... 100
Overload	F_x, F_y, F_z	kN	–7,5/7,5
F_z for F_x and $F_y \leq 0{,}5\ F_z$	F_z	kN	–7,5/15
Threshold		N	<0,01
Sensitivity	F_x, F_y	pC/N	≈–7,5
	F_z	pC/N	≈–3,7
Linearity, all ranges		%FSO	≤±1
Hysteresis, all ranges		%FSO	≤0,5
Cross talk		%	≤±2
Rigidity	c_x, c_y	kN/µm	>1
	c_z	kN/µm	>2
Natural frequency	$f_n(x, y, z)$	kHz	≈3,5 [4]
Natural frequency	$f_n(x, y)$	kHz	≈2,3 [3]
(mounted on flanges)	$f_n(z)$	kHz	≈3,5 [3]
Operating temperature range		°C	0 ... 70
Capacitance	F_x, F_y, F_z	pF	≈220
Insulation resistance (20 °C)		Ω	$>10^{13}$
Ground insulation		Ω	$>10^{8}$
Protection class EN60529		–	IP67 [3]
Weight		kg	7,3
Clamping area	mm	100x170	
Connection		Fischer flange, 9 pol. neg.	

[1] Application of force inside and max. 25 mm above top plate area
[2] Range for turning, application of force at point A
[3] With connecting cable Types 1687B5, 1689B5, 1677A5, 1679A5
[4] Without tool holder Type 9403

9257B_000-151e-11.09

Annex C

Plans of wings and joints. All the dimensions are expressed in mm.

Drawing 1: NACA 0012_A

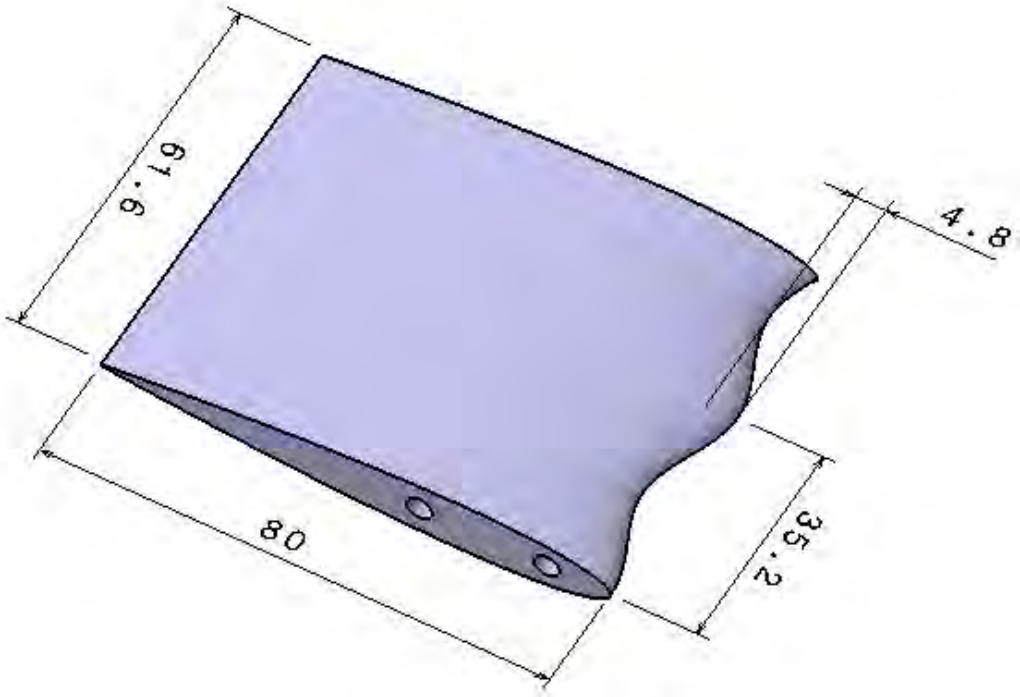

Drawing 2: NACA 0012_B

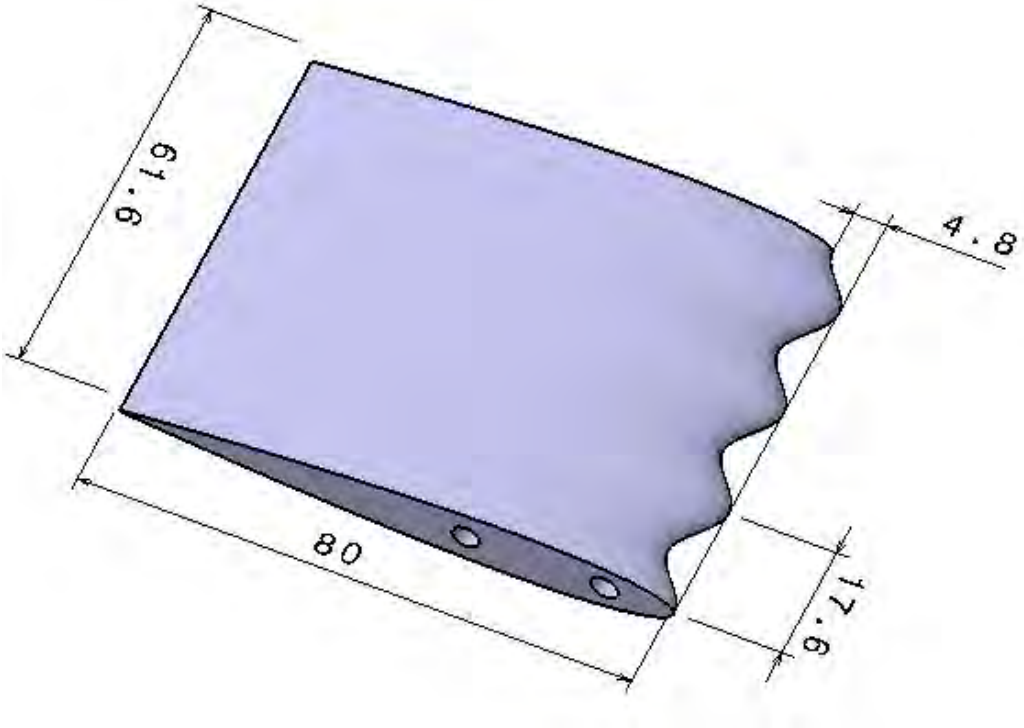

Drawing 3: NACA 0012_C

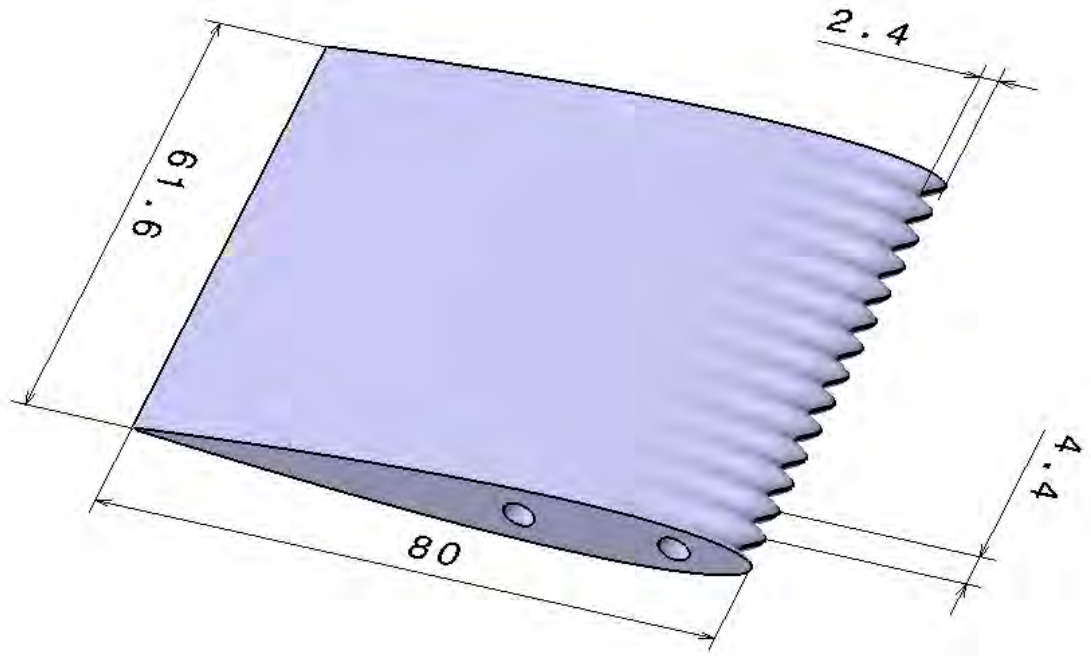

Drawing 4: Movable joint

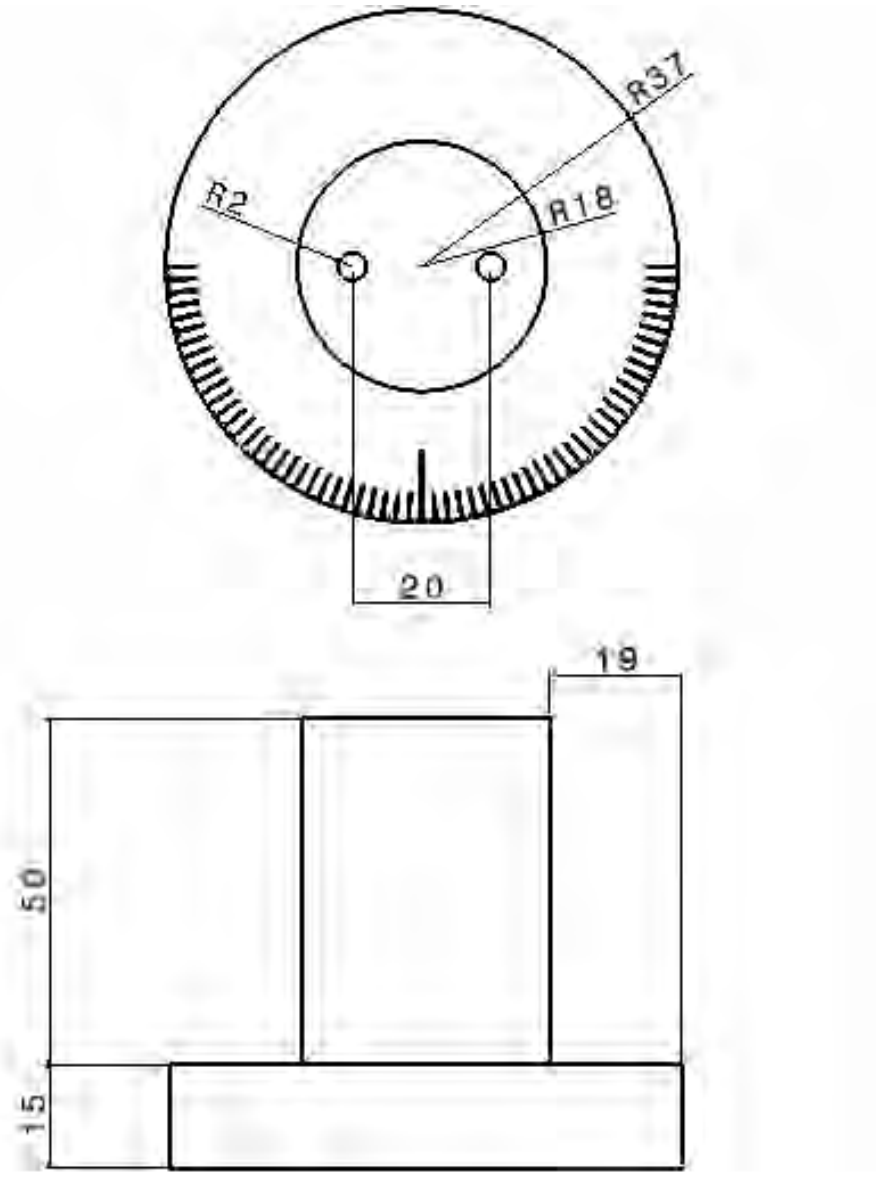

Drawing 5: Fixed joint